2018-06-01

Friction Bit Joining of Similar Alloy Sheets of High-Strength Aluminum Alloy 7085

Matthew R. Okazaki
Brigham Young University

Friction Bit Joining of Similar Alloy Sheets of High-Strength Aluminum Alloy 7085

Matthew R. Okazaki

A thesis submitted to the faculty of
Brigham Young University
in partial fulfillment of the requirements for the degree of

Master of Science

Mike P. Miles, Chair
Jason M. Weaver
Yuri Hovanski

School of Technology

Brigham Young University

ABSTRACT

Friction Bit Joining of Similar Alloy Sheets of High-Strength Aluminum Alloy 7085

Matthew R. Okazaki
School of Technology, BYU
Master of Science

Friction Bit Joining (FBJ) is a new technology used primarily in joining dissimilar metals. Its primary use has been focused in the automotive industry to provide an alternative joining process to welding. As automotive manufacturing has continually pushed toward using dissimilar materials, new joining processes have been needed to replace traditional welding practices that do not perform well when materials are not weld compatible. FBJ meets these needs perfectly as it provides strength as well as the ability to join materials of almost any kind.

The purpose of this research was to explore different applications of the FBJ process. Traditionally FBJ has used a steel bit to drill through a thin piece of aluminum and weld to a piece of steel behind the aluminum. This research explored a different application of FBJ by using a steel bit to drill through multiple pieces of aluminum and weld to a small steel bit on the backside of the aluminum. The primary goal of this research was to answer two questions. (1) How does drilling impact peak weld strength and (2) Does an optimal shank diameter exist in terms of peak weld strength?

As in other research, no universal parameters were found for optimization of lap shear, cross tension and t-peel tests. Drilling was found to be an important factor in peak weld strength. Number of flutes on the consumable steel bit was varied to see the impact of better and worse chip clearance ability. Increasing number of flutes was found to positively impact peak weld strength to a point. Optimal number of flutes was found to be different for each type of testing.

It was found that there was an optimal bit head to bit shank diameter ratio that optimized peak weld strength. Again the optimal diameter was different for each test. Bits of different diameters were created and then tested to measure the impact of varying shank diameters on peak weld strength. It was found that there was a strength tradeoff between two localized joint areas in diameter testing. Decreasing the shank diameter increased the amount of overlap formed by the bit head over the top coupon. This shifted strength to the bit head region. While this strengthened the bit head region of the joint, strength was sacrificed in the bit-nut intersection. This tradeoff was consistently found in all test types.

Keywords: FBJ, aluminum, automotive manufacturing, Matthew R. Okazaki

ACKNOWLEDGEMENTS

There are many people who have contributed to my education culminating in this thesis. First, I would like to thank Dr. Mike Miles for being a friend, mentor and my committee chair. His guidance and support was absolutely necessary for the success of this thesis. In addition to Dr. Miles, I appreciate the willingness and support rendered me by my graduate committee specifically, Dr. Yuri Hovanski and Dr. Jason Weaver. Student support in this project was also a key factor in my success. Multiple graduate and undergraduate students lent a hand and their expertise. In particular, Kevin Shirley, Shane Wood or Eliza Snyder.

Finally I wish to also acknowledge my family and their efforts and sacrifices in helping me complete my degree. I have been inspired my whole life by what my grandparents have been able to accomplish in their respective lifetimes. Whether it was overcoming racism, providing leadership in the LDS church or, more applicably, typing their own thesis' on a typewriter in a bathroom in a small apartment late into the night. My parents were the ones who originally instilled within me an understanding of the importance of education and then supported me in my pursuit of higher learning. The person I am today and all of my successes can trace their roots back to my parents guiding influence and support. I'd like to recognize my children, Eddie and Alta, for having been instrumental in providing motivation for this degree. My hope has been that through this education, I will be able to provide as good an upbringing for them as my parents provided for me. Lastly, I'd like to thank my wife Ally. Without her none of this would be possible. She has supported me financially, academically and emotionally throughout this whole journey. I can hardly begin to summarize the many sacrifices she has made that has allowed me to complete my degree.

TABLE OF CONTENTS

LIST OF TABLES

LIST OF FIGURES

1 INTRODUCTION

1.1 Background

The automotive industry is under constant pressure for innovation in all forms. Consumers want new functions and features that can only come with adoption or innovation of new technological advances. In addition to new technologies, consumers also want cars safer, more economical to operate and cheaper. The term made famous by renowned business mind Peter Drucker has become the unofficial automotive industry motto, “innovate or die”. In response to the consumers demand for innovation, the auto industry has responded with a barrage of investments. Investments have been made in research and development labs, consumer insight groups as well as process innovation centers. This research is a direct result of that investment in innovation.

Material selection has played a large role in automotive innovation. The introduction of Henry Ford’s Model T solidified steel as core material used in automotive manufacturing. Since the Model T, there has been a consistent push to make automobiles stronger and lighter. This has led to some major innovation. Audi introduced a new space frame technology in the A8 which utilized aluminum rather than steel as the primary material. Additionally, many companies are combining multiple materials such as steel alloys, aluminum alloys and polymers in the same car in order to achieve this goal of stronger and lighter. These new material combinations in car frames has created challenges in how to effectively join dissimilar materials (Stein & Dilthey, 2006).

Friction bit joining (FBJ) was developed as a method to effectively join dissimilar materials (Miles, et al., 2009). Common methods of joining in use are resistance spot welding (RSW), clenching and self piercing riveting (SPR) (Lim, et al., 2015). This research is a continuation in the development of the FBJ process. This research explores the expansion of the FBJ process to welding a consumable bit to a nut backing behind the two materials being joined rather than directly to one of the joining materials.

1.2 Objective

The objective of this research is to begin to investigate other application for the FBJ process. Much of the progress that has been made in developing FBJ as a process, has focused on joining two dissimilar materials, one of which is stir weld compatible with the consumable bit. This research focuses on expanding the application of FBJ beyond the constraint of having to have one of the joined materials be stir weld compatible with the bit. The objective is to use a nut backing, instead of the second material, that can be joined with the bit to form a joint.

1.3 Research Questions

There are a few major differences in the FBJ process that this research will be exploring when compared with the existing research. The first is that because we are not welding to the second material coupon we will have to drill through it. Thus drilling will be a more important function in this process than it was previously. This will necessitate changes in design to the bit. The question this research seeks to answer is: how does the drilling function of the FBJ process affect peak weld strength?

Secondly, in this research we anticipate that the primary weld failures will be classified in one of three categories. First, the consumable bit head will pull through the top coupon known as

a head pull through (HPT). Second a nugget from the nut where the consumable bit is joined will pull out causing the weld to fail known as a nugget tear out (NTO). Lastly the shank of the consumable bit could fail splitting in two. This is known as a shank failure (SF). The question this research tries to answer is: does an optimum shank diameter to head diameter ratio exist in terms of maximum peak weld strength?

1.4 Hypotheses

1. Increasing number of flutes, to a point, will have a positive impact on peak weld strength due to the improved ability of the bit to clear chips, after which the effect will be null or even detrimental.
2. Decreasing bit shank diameter, to a point, will have a positive impact on peak weld strength due to the bit having to cut through less material mass prior to the welding phase. After the shank diameter inflection point has been reached it will have a deteriorating impact on peak weld strength.
3. There is an optimal ratio between consumable bit head diameter and consumable bit tip surface area that will lead to the greatest amount of peak weld strength.

1.5 Methodology

1.5.1 Materials

Two materials were used in experimentation. 2 mm thick AA7085 was used to make the coupons that were joined together. 4140 annealed steel was used to make both the consumable bit and the consumable nut used in the welding process. In all weld types, the consumable bit

pierced both aluminum coupons and then was joined to the consumable steel nut on the backside via friction stir welding as show in Figure 1-1: Generic Representation of a Weld.

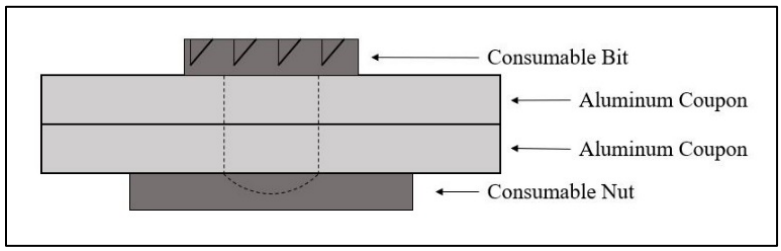

Figure 1-1: Generic Representation of a Weld

Lap shear, cross tension and t-peel tests were run on each bit design to determine peak weld strength. See Figure 1 2: Lap Shear Coupon Drawing and Figure 1 3: Lap Shear Overlap Coupon Drawing for dimensions and testing set up respectively.

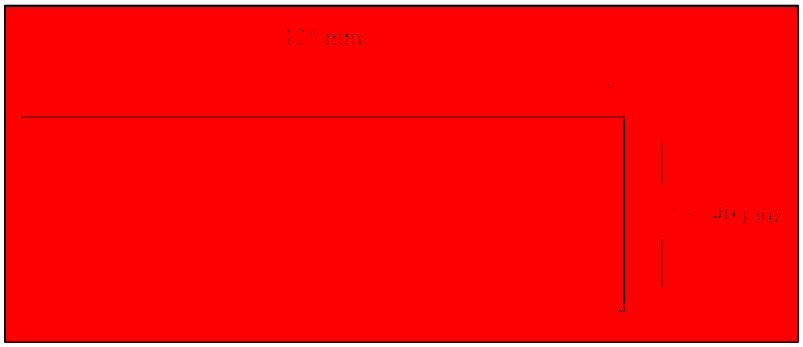

Figure 1-2: Lap Shear Coupon Drawing

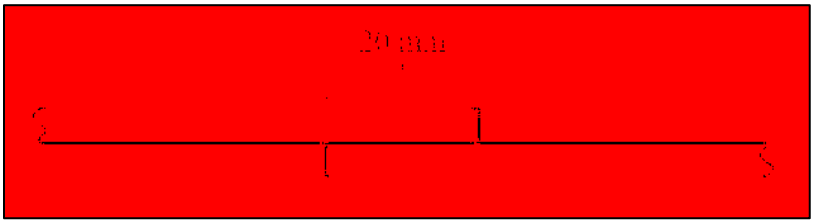

Figure 1-3: Lap Shear Overlap Coupon Drawing

Coupons for the cross tension test were 150 mm by 50 mm with 20 mm holes drilled 25 mm from each end of each coupon as seen in Figure 1-4: Cross Tension Coupon Drawing. When joined, both coupons were placed on top of each other with a 90-degree offset with centers aligned as seen in Figure 1-5: Cross Tension Coupon Overlap Drawing. Coupons were cut individually and then stacked and drilled in a batch.

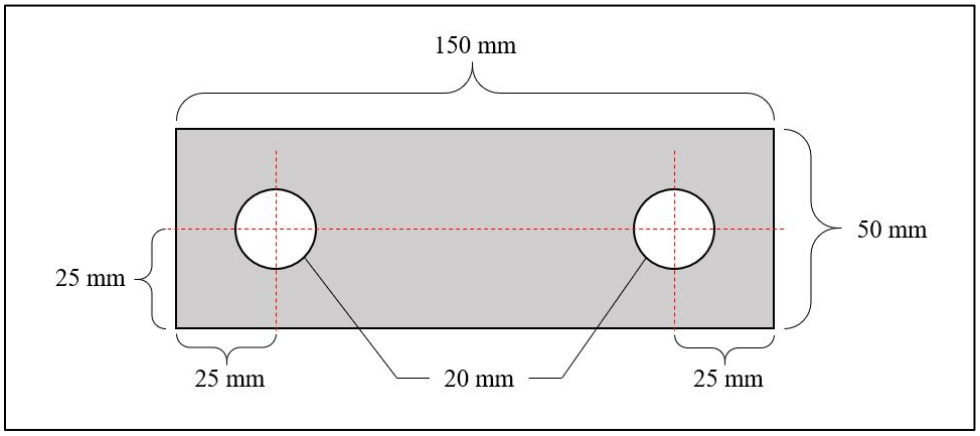

Figure 1-4: Cross Tension Coupon Drawing

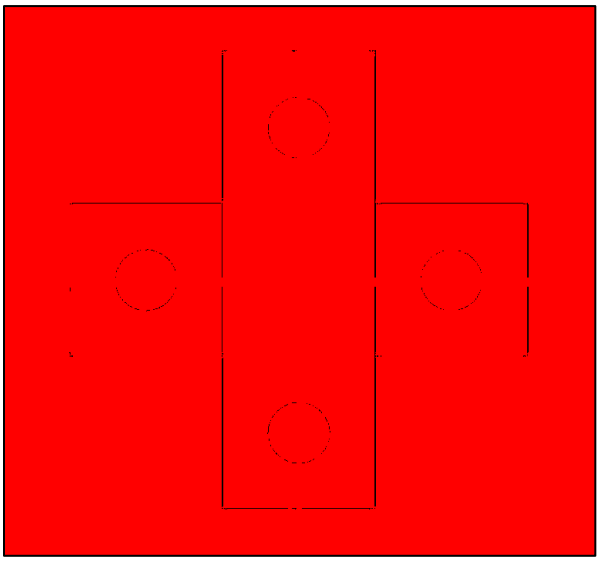

Figure 1-5: Cross Tension Coupon Overlap Drawing

Coupons for the t-peel tests were the same blank size as were the lap shear test (see Figure 1-2: Lap Shear Coupon Drawing), however were bent at a 90-degree angle with a 5 mm internal radius 35 mm from one end as shown in Figure 1-6: T-peel Coupon Drawing. T-peel coupons were butted up short end to short end with a 180-degree rotation prior to welding as shown in Figure 1-7: T-peel Coupon Overlap Drawing.

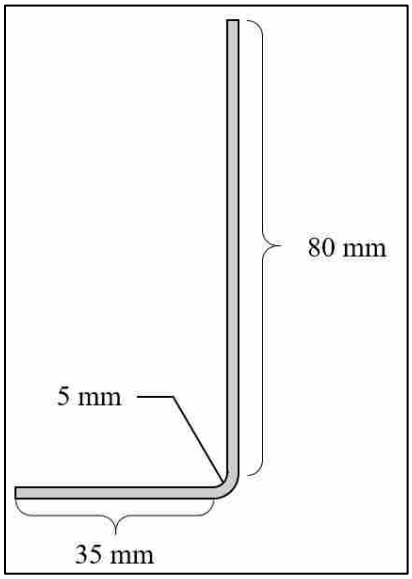

Figure 1-6: T-peel Coupon Drawing

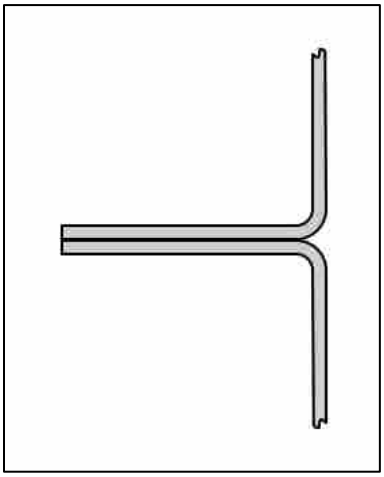

Figure 1-7: T-peel Coupon Overlap Drawing

Consumable bits were made of 4140 annealed steel using a CNC lathe, die set, grinding belt and 25-ton hydraulic press. Consumable bits were cut out of 4140 rod stock. The consumable nut was also made out of 4140 annealed steel using a CNC lathe. Consumable nuts were cut out of 4140 hex stock.

Joints were made using a prototype FBJ machine originally designed by MegaStir Technologies and later modified by the Brigham Young University Precision Machining Lab and members of the FBJ research team.

1.5.2 Experiments

In order to answer the research questions posed earlier, a series of experiments was performed involving destructive testing of FBJ samples. Samples were pulled in tension using the lap shear, t-peel and cross tension testing methods in the Brigham Young University Instron machine. Test samples were made using the prototype FBJ weld machine.

While there were a great deal of independent variables that could be manipulated, the scope of this research required that we focus on only and handful of the many possible options. An initial baseline scenario was established early on in the research process against which each trial would be compared. Once the baseline test was set, all other parameters were frozen while a single parameter was tested at a time. All parameters other than shank diameter and number of flutes were frozen before the baseline sample had been collected.

Other parameter such as, but not limited to, Z-depth, RPM, Z velocity, dwell time, nut size and shape, and clamping pressure were determined prior to the baseline test using a variety of methods. The objective of setting these other parameters was not to optimize results but rather

to establish a consistent repeatable process that would minimize the noise in the subsequent design of experiments (DOE).

In each iteration of the DOE a single independent variable was changed and fifteen to sixteen samples were collected for each of the three tests, lap shear, cross tension and t-peel. Results were recorded and compared against the baseline to determine whether or not the results supported the researches hypotheses.

1.6 Delimitations and Assumptions

Only two materials were used in our experimentation set. Materials other than 4140 annealed steel for the consumable bits and AA7085 for the joining coupons were not considered.

Additionally, each sample was completely custom made. Each bit and coupon were made individually by the FBJ research team. While the machining skills of the FBJ team were acceptable, it should be noted that they still do match the consistency and accuracy of a professional machinist and certainly not that of a fully automated, well-tuned process. As such, there is bound to be more variation between samples due to differences in physical characteristics than would be typical found in a fully automated process.

Finally, while the FBJ prototype machine was capable of running the trials that the research called for, there were some deficiencies in the machine design itself that forced us to compensate using machine settings. One known example of this was the lack of stiffness in the frame. We noticed that during welding, deflection would take place due to the extreme amount of force required to plunge the consumable bit into the aluminum alloy coupons. This deflection was offset by adjusting some of the welding parameter. This deficiency in machine design and

subsequent compensation with machine parameters may make it difficult for third parties to repeat this researches results using the same testing parameters presented here.

1.7 Glossary

DOE – Design of Experiments: method through which multiple independent variables can be tested and compared individually.

FBJ – Friction Bit Joining: process using a consumable bit to spot join sheet metal by drilling through the top layers and friction-welding to another piece of metal acting as a backing.

HAZ – Heat Affected Zone: zone of the weld which is heated and cooled rapidly.

HPT – Head Pull Through: failure mode by which the head of the consumable bit pulls through the top piece of the aluminum alloy.

NTO – Nugget Tear Out: failure mode by which the weld area of the FBJ process tears out a chunk of metal (nugget) from the joint backing.

RPM – Revolutions Per Minute: a metric used to measure the speed of a spinning object or tool.

RSW – Resistance Spot Weld: A fusion-welding process that uses electrodes to clamp the sheet metal pieces together and pass a current through them which produces the necessary welding heat.

SF – Shank Failure: failure mode by which the shank of the consumable bit fails causing the joined pieces of aluminum alloy to separate.

SPR – Self Piercing Rivet: A cold joining process that uses a die set to force a rivet into sheet metal without predrilling a hole

STD – Standard Deviation: A measure of dispersion of a group of samples from its mean.

UHHS – Ultra High Strength Steel

2 LITERATURE REVIEW

2.1 Introduction

The focus of this research on a larger scale is to pioneer new technology that will have application in joining dissimilar metals that make typical processes such as welding difficult to effectively implement. The review of current literature focuses on these competing technologies with a brief analysis of their strengths and weaknesses.

2.2 Change in the Auto Industry

The need for innovation in the automotive industry comes from a variety of sources. Consumers are constantly demanding new and better features in their vehicles. Competitors within the industry are creating pressure to keep up or stay ahead of the field. Finally, government regulation is additionally shaping the industry. All three of these forces are driving the need for lighter weight vehicles. The consumer is demanding better gas mileage, the competition is innovating new lighter vehicles that bring a whole host of competitive advantages to their business and the government is demanding that vehicles meet specified fuel efficiency standards.

The Corporate Average Fuel Economy (CAFE) regulations have put pressure on the auto industry by the government to produce a fleet of cars more fuel efficient than ever before. While there are different ways to meet the increasingly higher standards, light weighting of vehicles is one of the major focuses. A study conducted by DuPont reveals that light weighting is a major

focus for fuel efficiency improvement in the automotive industry. See Figure 2-1: DuPont Study of Fuel Efficiency Study Foci (DuPont, 2014).

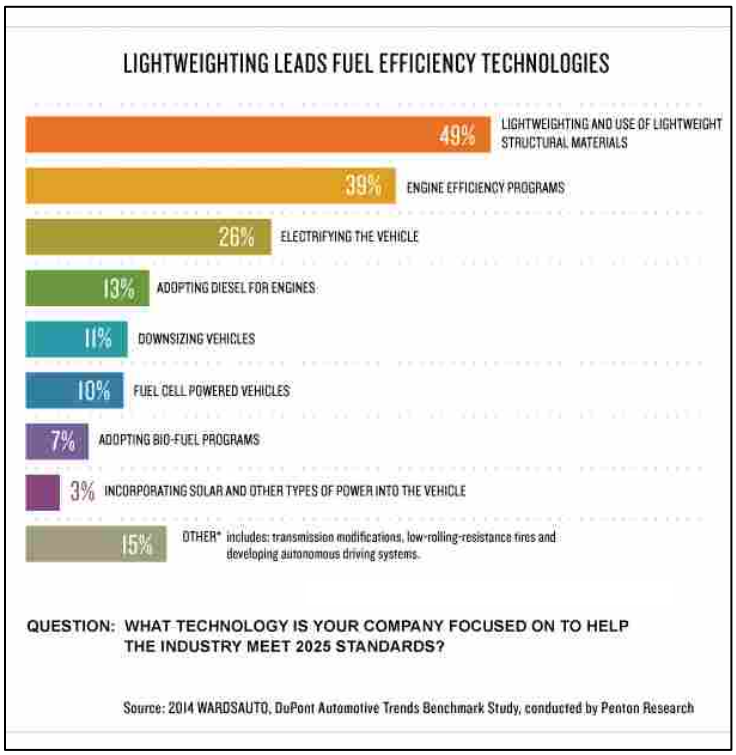

Figure 2-1: DuPont Study of Fuel Efficiency Study Foci

One movement in the pursuit of lighter vehicles that is gaining increasing momentum is the use of light weight, high strength materials. As referenced earlier Audi was a pioneer in this field creating the first vehicle to use aluminum alloy as the primary material for the frame of the car (Stein & Dilthey, 2006). While Audi may have been the first, many other car manufacturers have followed suit. Ford's F-150 was designed and built around an aluminum intensive body. BMW's I3 was similarly built around a non-steel body of carbon fiber, aluminum alloys and polymer plastics (Deptula & Noah, 2015).

The challenges of using lightweight alloy material have been considerable. One particular area which has caused problems for automotive manufactures wishing to use weight saving dissimilar metals is the joining process. Compatible metals are able to be joined using traditional technology such as spot welding, whereas dissimilar metals are not able to be joined using traditional techniques (Miles, et al., 2009). Certainly carbon fiber and polymers fall into this category as well.

A technology that has emerged as a solution to this problem is FBJ. FBJ has proven to overcome many of the shortcomings of current dissimilar metals joining processes and to be a viable options for many joining operations (Squires, Lim, Miles, & Feng, 2015). The FBJ process traditionally has used a consumable bit to pierce through a single sheet of and aluminum alloy and the create a weld between the consumable bit and a piece of ultra high strength steel (UHSS) behind the aluminum. This research seeks to expand upon that research and add value to the FBJ process through exploring how the FBJ process performs in application where material thickness is greater than what has been tested, as well as applications where more than two sheets of metal are being joined.

2.3 Resistance Spot Welding

Resistance Spot Welding is a technique that uses a higher current of electricity to fuse two working pieces together. Two working pieces of similar metal are clamped together by two copper electrodes. A current is passed from one electrode through the clamped work pieces to the other electrode. The electrical current and resistance of the work piece create the heat necessary for fusing the two work pieces together via a weld (Nied, 1984). See Figure 2-2: RSW Example Diagram.

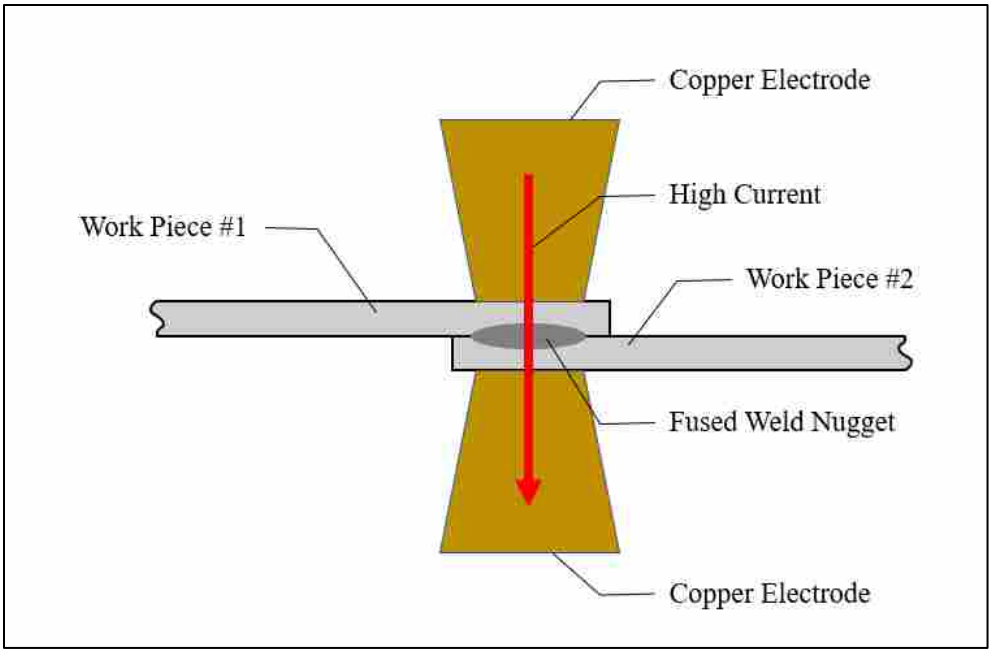

Figure 2-2: RSW Example Diagram

RSW of aluminum presents a particularly difficult challenge to the RSW process. The RSW process relies on the resistance of the metal between to the electrodes to create the heat necessary to create the fusion between the two pieces being joined. This method works quite well with mild steels as there is sufficient resistance at lower currents to generate the necessary amount of heat. However, aluminum runs into problems with this method due to a significantly higher thermal and electrical conductivity. These two properties that often make aluminum an attractive material, end up working against it in RSW. Because of its ability to conduct electricity and its ability to disperse heat, significantly higher currents are needed to generate the required heat to form the weld (Hao, Osman, Boomer, & Newton, 1996). Aslanlar found that for welding steels, 8.5 kA was sufficient to produce a satisfactory weld (Aslanlar, 2006) while Florea et al. found that they needed 26 kA to produce good results (Florea, et al., 2012).

Experiments have been carried out joining two 1 mm thick coupons of 6082-T6 aluminum through the RSW process. These experiments were successful and able to achieve individual peak weld strengths of up to 3.4 kN when tested in a lap shear configuration. Multiple variables were tested in order to achieve optimized peak strength in this configuration. Thirteen scenarios were run in total with sample sizes of four samples each. The results look consistent, however the low sample size lacks statistical significance (Pereira, Ferreira, Loureiro, Costa, & Bartolo, 2009)

Additionally, research completed by Sun et al. tested the RSW process of 2 mm thick coupons of both 5182-O to 5182-O aluminum alloy and 5182-O to 6111-T4 aluminum alloy. Sun et al. tested peak loads of both of these joining combinations under lap shear, cross tension and t-peel conditions. See the results of this research summarized in Table 2-1: Summary of RSW Results (Sun, Stephens, Davies, Khaleel, & Spinella, 2004).

Table 2-1: Summary of RSW Results

	5182-O to 5182-O	5182-O to 6111-T4
Lap Shear	7.16 kN	7.17 kN
Cross Tension	6.05 kN	5.95 kN
T-Peel	1.34 kN	1.37 kN

The research by Sun ran 30 specimens per parameter settings. Results are incredibly consistent and provides an extremely good data set against which we can compare our results.

2.4 Clinching

Clinching is a mechanical binding process for joining two pieces of metal. It relies on mechanical binding as a source of its strength. A clinched joint is formed by use of a punch and a

device to hold the material as shown in Figure 2-3: Clinching Process Diagram. The punch mechanically deforms the joined pieces and in the process metal is interlocked forming a mechanical hold (Varis & Lepisto, 2003).

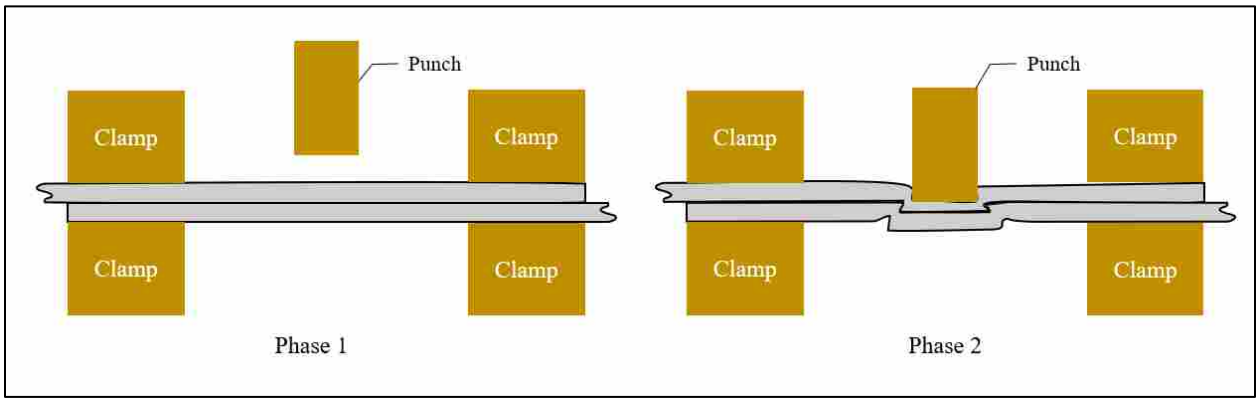

Figure 2-3: Clinching Process Diagram

Clinching has a distinct advantage of being more economical than other forms of joining due the lack of extra consumable material used in the process. Unfortunately, however, it is also one of the weaker forms of joining processes. Lap shear and cross tension tests were run by Chen et al. They tested multiple variations of material type and clinching techniques. A summary of their best results can be seen in Table 2-2: Summary of Clinching Results The joint type for these tests was a height-reduced clinched joint with AL6061 as the top coupon and AL5052 as the bottom coupon (Chen, Zhao, Han, Cui, & Fan, 2016).

Table 2-2: Summary of Clinching Results

	Peak Strength
Lap Shear	3.0 kN
Cross Tension	1.3 kN

The peak strengths for the lap shear and cross tension tests are quite low when compared to other joining methods. Additional studies have been done on clinched joints. Like most of the processes discussed in this research, adhesive bonding can be added to generally increase peak strength. In tests run on aluminum alloy 7075 lap shear tests were run with and without a bonding adhesive. Results of this research is summarized in Table 2-3: Summary of Bonded vs Unbonded Peak Strength (He, et al., 2014).

Table 2-3: Summary of Bonded vs Unbonded Peak Strength

	Clinched Joint	Clinched/Bonded Hybrid Joint
Lap Shear Tests	2385 N	2431 N

While the maximum strengths are still low in comparison to other joining techniques it is clear that the addition of adhesives can improve overall peak strength.

2.5 Self Piercing Rivets

SPR is a cold forming process that uses a consumable rivet to bind two working pieces together. The rivet itself has a circular head with two legs. In the riveting process the legs are forced through the top working piece by a driver applying pressure to the head. The top sheet is punctured and then the legs continue downward into the bottom working piece. The design of the rivet is such that rather than puncture the bottom piece as well, the bottom piece is deformed with the rivets legs. Deformation of the bottom working piece and rivet is controlled with the use of a die positioned opposite the driver. This controlled deformation forms a mechanical bind joining the rivet with the working pieces (Porcaro, Hanssen, Langseth, & Aalberg, 2006). See Figure 2-4: Riveting Process Diagram for an example of the riveting process.

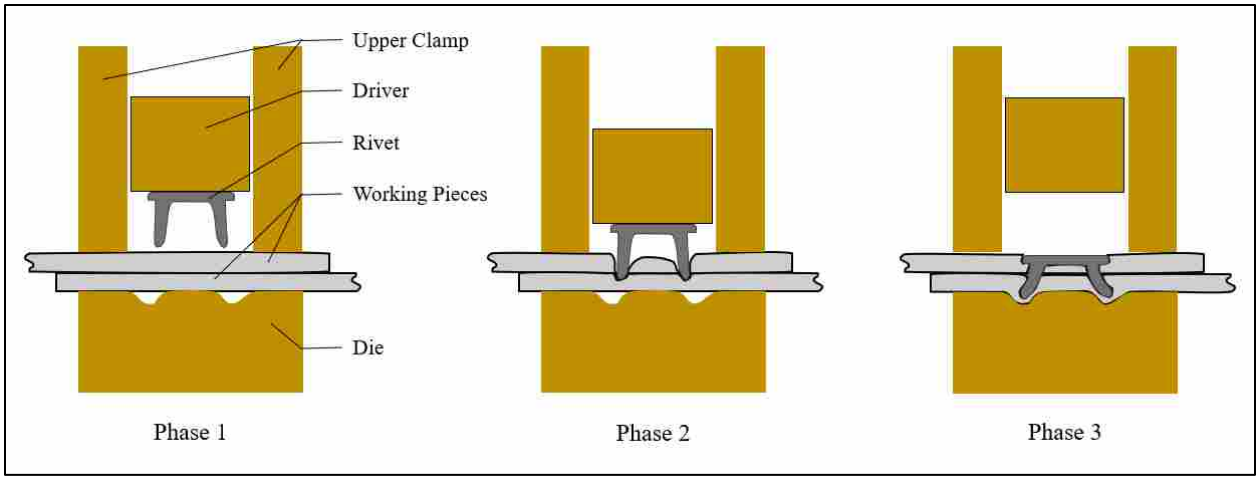

Figure 2-4: Riveting Process Diagram

SPR technology is viewed as an alternative to welding. SPR is fairly economical and is able to achieve relatively high peak strengths. Testing of 2mm thick AA5754 coupons revealed peaks strengths in the lap shear and cross tension configurations significantly less than those observed in the RSW process, however T-peel sample peak strengths exceeded those of RSW (Han, Thornton, & Shergold, 2010). See Table 2-4: Summary of SPR Peak Strengths. Additionally it has been found that the SPR process does significantly better the RSW process under fatigue testing (Wang, Hao, Zhang, & Zhang, 2005).

Table 2-4: Summary of SPR Peak Strengths

	Peak Strength
Lap Shear	5.0 kN
Cross Tension	3.7 kN
T-Peel	2.1 kN

While the lap shear and cross tension tests were lower than results obtained by the RSW process, the t-peel test of the SPR joint exceeded those of the RSW joint. It has been found in

similar experiments that there is no single universal weld setting that optimizes all three tests simultaneously (Shirley, 2018). Because a process must pass all three of these tests in order to be used in auto manufacturing, it is advisable to optimize for the weakest of the three. RSW exceeds the results obtained by SPR in every category except that of t-peel. Unfortunately for RSW, the t-peel values are below the target of 1500 N for a single joint while the SPR process surpasses the target 1500 N in the t-peel test. Although SPR does well in t-peel it does not do well in lap shear, achieving an average of only 5000 N which is the minimum threshold for that test.

SPR can also be used with the addition of adhesive bonding to increase joint strength. In a separate study, the addition of adhesive to an SPR joint was studied in how it relates to joint strength. It was found that the adhesive joint strength and the SPR joint strength was essentially additive (He, Xing, Zeng, Gu, & Ball, 2013). See Table 2-5: Summary of Adhesive/SPR Joint Hybrid Study.

Table 2-5: Summary of Adhesive/SPR Joint Hybrid Study

	Peak Strength
Adhesive Joint	397 N
SPR Joint	2646 N
SPR/Adhesive Hybrid Joint	3071 N

3 METHODOLOGY

3.1 Overview

The focus of this research was how bit design affected peak weld strength in applications where drilling was of greater importance due to thicker joining pieces. As such, the process for this research was as follows:

1. Adaptation of existing previous FBJ designs and tooling was necessary to accommodate the additional joining material thickness and nut. Additionally, new parts and consumables needed to be produced for the research trials.
2. Modification of the existing FBJ process was completed to find suitable weld parameters which we could use in order to run our trials.
3. Trials were conducted testing several different hypotheses in which data was collected.
4. Collected data was analyzed.
5. Results, conclusions and recommendations were compiled.

3.2 FBJ Design and Tooling Adaptation

Brigham Young University has been conducting research on the FBJ process since 2006. The FBJ process has come a long way since then. This research is the latest iteration of the research that has been previously conducted. In order to make this research feasible it was necessary to modify and enhance existing designs and equipment to fit the needs of this research.

Additionally parts and consumables needed to be produced in order to conduct trials. Necessary modifications and produced parts and consumables include:

1. FBJ welding machine
2. Consumable bit design
3. Consumable bit driver
4. Consumable bits
5. Consumable nuts
6. Test sample coupons
7. Experimental design

3.2.1 FBJ Welding Machine

The machine used for the welding process was a prototype machine made by Megastir. The machine is essentially a servo motor and driver assembly attached to a frame with a table, clamping device and load cell. See Figure 3-1: FBJ Welding Machine.

Figure 3-1: FBJ Welding Machine

The majority of the machine required no modification from the original state. The only part that needed to be modified was the table. In the original state the table did not have the sufficient clearance to allow a nut to fit under the two samples when the samples were clamped together in preparation for welding. See Figure 3-2: FBJ Welding Table.

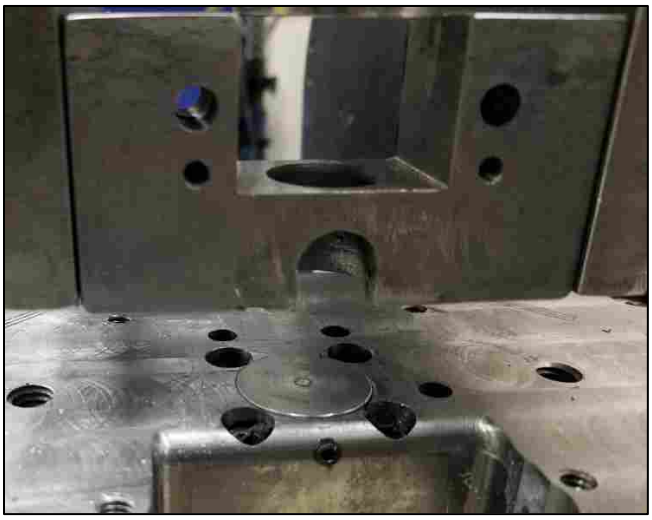

Figure 3-2: FBJ Welding Table

In order to allow clearance for a nut to fit under the clamped sample, a recess was cut into a new puck for the table assembly as seen in Figure 3-3: Puck with Recess.

Figure 3-3: Puck with Recess

A new puck needed to be manufactured. This was done using D2 tool steel and a Fryer CNC lathe as seen in Figure 3-4: Fryer CNC Lathe.

Figure 3-4: Fryer CNC Lathe

One of the difficulties with cutting the recess in the puck was that the centerline of the servo motor and driver assembly was not concentric with the centerline of the puck. Thus the recess needed to be cut offset to the center. This was done by making an initial “best guess” as to where the recess should be located on the puck. The recess was cut using a standard drill press with 1/8” end mill and 1/8” drill for pocketing the corners. See Figure 3-5: Acer Drill Press.

Figure 3-5: Acer Drill Press

While our initial guess was good enough to make a weld it was still significantly off center as seen in Figure 3-6: Off-Center Weld.

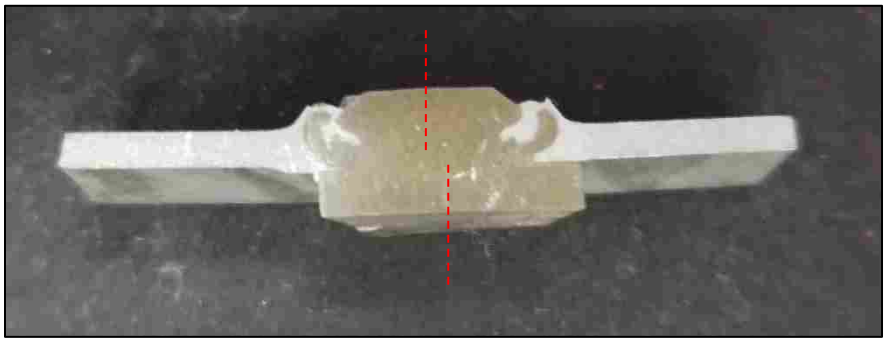

Figure 3-6: Off-Center Weld

Center alignment was accomplished by making a weld then using an optical comparator (See Figure 3-7: Optical Comparator) to measure the offset distance. This distance was then used to adjust the recess location in the puck allowing us to align bit and nut centerlines for welding. See Figure 3-8: Centered Nut. The final pocket was machined using a custom program for a Fryer CNC machine, see Figure 3-9: Fryer Mill.

Figure 3-7: Optical Comparator

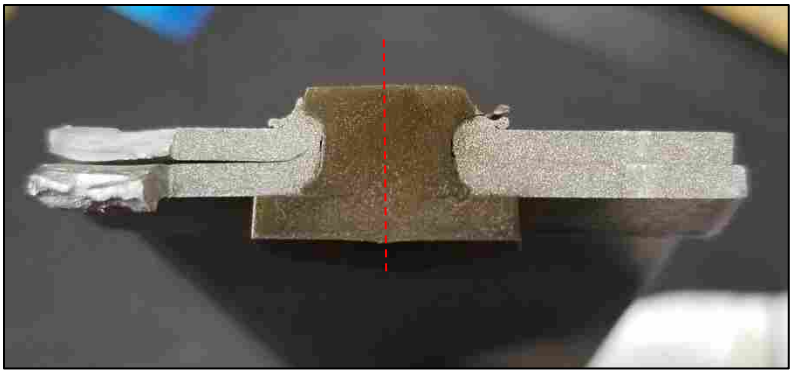

Figure 3-8: Centered Nut

Figure 3-9: Fryer Mill

Once the nut and bit centerlines were concentric and the pocket was recessed into the puck, the FBJ machine was ready to start making testable welds.

3.2.2 Consumable Bit Design

Thanks to prior research, a consumable bit design already existed and was used as a starting point for this research. The original design consisted of a circular head with driving

features and a short shaft with two flutes for cutting features. All bits had a 0.300” head diameter. See Figure 3-10 : Original FBJ Bit Design.

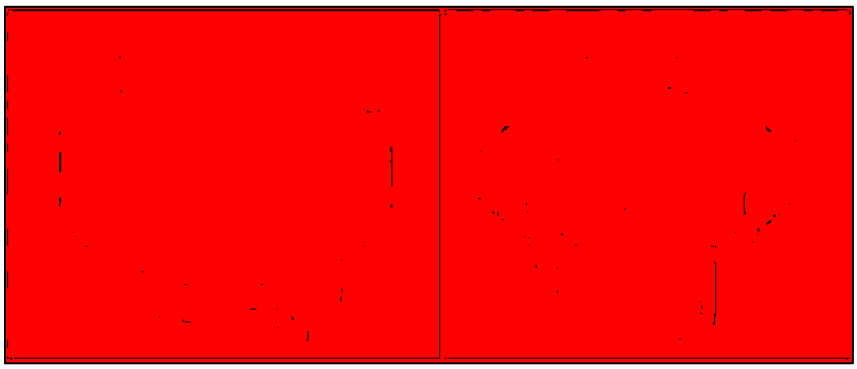

Figure 3-10 : Original FBJ Bit Design

The major modification to the bits was that the shaft length needed to lengthened to accommodate for the added material the bits would be cutting through. In the end six different major bit variants were produced.

ECHO6: See Figure 3-11: ECHO6 Bit – This was the first bit produced and tested in a full set of fifteen samples. This bit had an elongated shank as compared to the original bit design as seen in Figure 3-10 : Original FBJ Bit Design. Additionally this bit had no flutes or cutting features. The original purpose of this bit was to act as a baseline against which we could test our samples. Once the results of the this sample was collected it was deemed that the standard deviation of this sample set was too great to act as a good baseline. The STD was 2020 N which was +/- 26% of average peak strength in lap shear testing. Further design changes were necessary to reduce the STD. Ultimately cutting features and flutes were added in the ECHO9 variant that reduced STD to an acceptable level to serve as a baseline test. Due to the high STD, ECHO6 was only tested in the lap shear configuration.

Figure 3-11: ECHO6 Bit

ECH09: See Figure 3-12: ECHO9 Bit – Modification to ECHO9 included a slightly shorter total length (ECHO6 was 0.473”, ECHO9 was 0.423”) as well as the addition of two flutes and cutting features. ECHO9 STD was 345 N or roughly +/-3% of average peak strength in the lap shear test. Due to the tighter STD results, ECHO9 was chosen to act as a baseline.

Figure 3-12: ECHO9 Bit

ECH10: See Figure 3-13: ECH10 Bit – Modification was limited to number of flutes. ECH10 was equipped with a total of three flutes at 120-degree intervals.

Figure 3-13: ECH10 Bit

ECH11: See Figure 3-14: ECH11 Bit – Modification was limited to the shank diameter size. Flute depth also needed to corrected due to the different shank size. ECH11 shank diameter was decreased to 0.220 in. Additionally flute depth of cut was reduced by 20% maintaining roughly the same flute size to diameter ratio as the ECHO9 bit variant.

Figure 3-14: ECH11 Bit

ECH12: See Figure 3-15: ECH12 Bit – Modifications included a combination of changes made to both ECH10 and ECH11. Number of flutes was increased from two at 180-degree

intervals to three at 120-degree intervals. Shank diameter was decreased from 0.280 in to 0.220 in. Additionally flute depth of cut was reduced by 20% maintaining roughly the same flute size to diameter ratio as the ECHO9 bit variant.

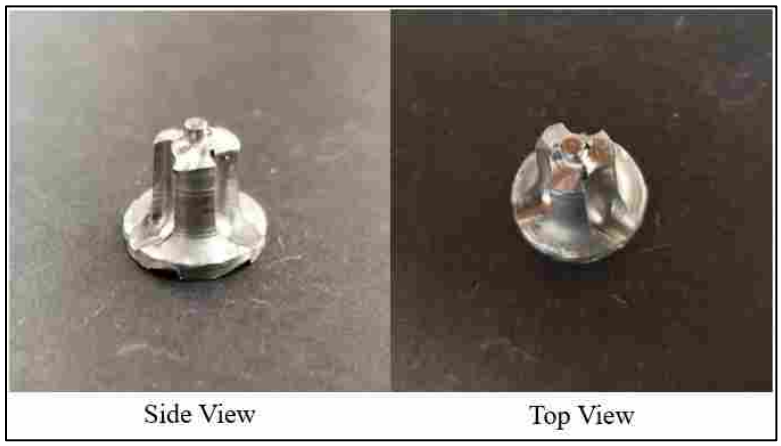

Figure 3-15: ECH12 Bit

ECH13: See Figure 3-16: ECH13 Bit – Modifications were limited to shank diameter size. The shank diameter size for this bit variant started at 0.250” at the nose and flared to 0.270” at the start of the head radius.

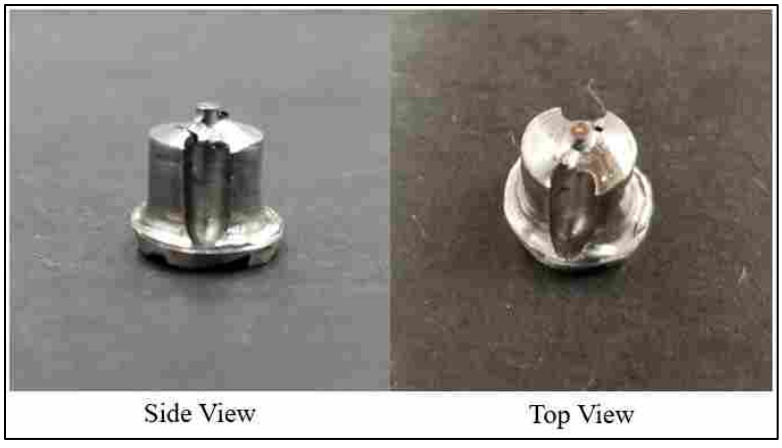

Figure 3-16: ECH13 Bit

3.2.3 Consumable Bit Driver

The driver was a key component in the welding process. The driver consisted of a mirror image teeth set to that of the bit as well as a small magnet imbedded in the driver itself. The magnet held the bit in place on the driver prior to engagement with the sample coupon. The outside of the driver was sleeved in a ½" needle roller bearing. This allowed the driver to have a contact fit with the hole in the clamping block while still being uninhibited from rotating. See Figure 3-17: FBJ Driver Configuration. The teeth of the driver then engaged with the bit to drive the bit though the coupons into the nut. Over the course of the research it was necessary to manufacture several drivers as occasionally there would be a mishap in the welding process that would destroy a driver. There were two common failures. The first was when the bit flipped on its side in the driver prior to or upon contact with the test coupon. This resulted in the bit welding itself to the driver. See Figure 3-18: First Typical Bit-Driver Failure. The second common failure was when the teeth would not have proper engagement causing slippage which resulted in the bit welding itself to the driver as shown in Figure 3-19: Second Typical Bit-Driver Failure.

Figure 3-17: FBJ Driver Configuration

Figure 3-18: First Typical Bit-Driver Failure

Figure 3-19: Second Typical Bit-Driver Failure

Prior research had made some of these bearings available for use, however modification was needed. Diameters of the existing drivers was wrong and need to be corrected. Additionally the bearing, bushings and snap rings needed to be fit to the driver. All modifications were done using a standard manual lathe as shown in Figure 3-20: Manual Lathe.

Figure 3-20: Manual Lathe

3.2.4 Consumable Bits

Bit designs were produced using an Okuma CNC lathe as seen in Figure 3-21: Okuma Lathe. Bits were produced using 4140 annealed steel. All Okuma CNC code can be found in Appendix A.

Figure 3-21: Okuma Lathe

Once bits were cut from the lathe, the cutting features were pressed into them using a die set a hydraulic press. See Figure 3-22: Die Set and Figure 3-23: Hydraulic Press.

Figure 3-22: Die Set

Figure 3-23: Hydraulic Press

3.2.5 Consumable Nuts

Consumable nuts were cut from 15 mm hex stock of 4140 annealed steel. Nut height was 0.1 in. Consumable nuts were cut using a custom parting program on a Fryer CNC lathe as shown in Figure 3-4: Fryer CNC Lathe. The end result was a small hex nut that was able to be slotted under the stacked test coupons for the bit to weld to as seen in Figure 3-24: Hex Nut.

Figure 3-24: Hex Nut

3.2.6 Test Sample Coupons

Three separate coupon types were needed for each of the three tests. Production methods for each coupon varied based on requirements.

Lap shear: Figure 1-2: Lap Shear Coupon Drawing – lap shear coupons were produced using a large Accurl hydraulic shear as seen in Figure 3-25: Accurl Hydraulic Shear.

Figure 3-25: Accurl Hydraulic Shear

Cross Tension: Figure 1-4: Cross Tension Coupon Drawing – cross tension coupons were produced using a large Accurl hydraulic shear as seen in Figure 3-25: Accurl Hydraulic Shear. Once coupon blanks were cut, a Fosdick drill press, as seen in Figure 3-26: Fosdick Drill Press, was used with a ¾" drill to cut the holes required for the cross tension test method.

Figure 3-26: Fosdick Drill Press

T-peel: Figure 1-6: T-peel Coupon Drawing – t-peel coupon blanks were the same size and dimensions as were the lap shear coupons shown in Figure 1-2: Lap Shear Coupon Drawing. Thus t-peel blanks were cut using the same method as the lap shear coupons. Bending the coupons to the required 90-degree angle was done using a Grizzly 12: Pan & Box Break and a custom build bending jig as shown in Figure 3-27: Grizzly 12" Pan & Box Break. Prior to being bent coupon blanks were heated to 120-degrees Fahrenheit to improve ductility and decrease fracturing during the bending operations. The coupons were heated in an oven shown in Figure 3-28: Oven for Pre-Heating Coupons.

Figure 3-27: Grizzly 12" Pan & Box Break

Figure 3-28: Oven for Pre-Heating Coupons

3.2.7 Experimental Design

The purpose of this research was to test how the FBJ process performed under different circumstances. Specifically this research tested the drilling functions impact on peak weld strength. The experiment was designed to test two different independent variables that would have an effect on drilling.

First was the number of flutes each bit had. We hypothesized that increased number of flutes would have a positive impact on peak weld strength. In order to test this theory, we created two different bit designs. ECHO9 was the baseline design with two flutes and ECH10 was altered design with three flutes. All other independent variables were held constant in order to decrease noise in the results.

The second theory was that there is an optimal ratio between bit shank size and head size that would result in an optimal peak load. To test this theory three bit designs were created. ECHO9 was the baseline design as well as the upper limit with a starting diameter of 0.280". ECH11 was the lower limit with a starting diameter of 0.220" and ECH13 was positioned in the middle with a starting diameter of 0.250".

ECH12 was a combination of modification made to both ECH10 and ECH11. Specifically a decreased shank size with three flutes. The purpose of this bit design was to analyze whether or not the two independent variables had any interaction.

The goal was to create a minimum sample size of fifteen. For all experiments sixteen samples were run as a precaution in case we lost a sample during testing. In the majority of the testing, we did not lose a sample which is why our data sets consist of sixteen samples for most trials. A summary of each bit design can be seen in Figure 3-29: Summary of Bit Designs.

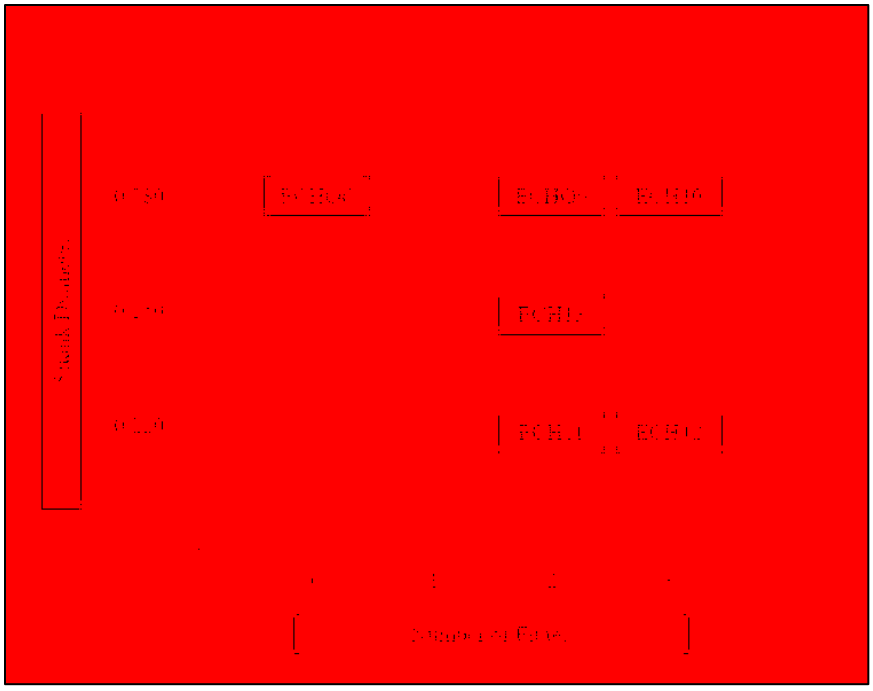

Figure 3-29: Summary of Bit Designs

3.2.8 Testing

Destructive testing was carried out on all test samples using an Instron machine, see Figure 3-30: Instron Machine. Samples were pulled in tension using a rate of 10.16 mm/min. Each sample type had slightly different configuration for testing.

Figure 3-30: Instron Machine

Lap shear was configured using the Instron's jaws to grab the sample with spacers to minimize bending moments within the sample. The force directions as well as gripping apparatus can be seen in Figure 3-31: Lap Shear Force Diagram and Figure 3-32: Instron Jaws for Lap Shear and T-Peel respectively.

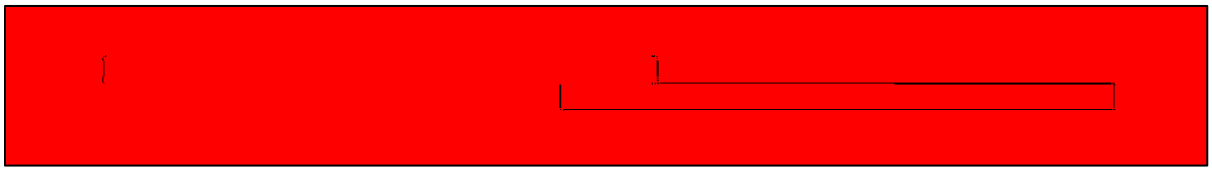

Figure 3-31: Lap Shear Force Diagram

Figure 3-32: Instron Jaws for Lap Shear and T-Peel

Cross tension was configured using custom made fixtures using a nut and washer combination to attach the sample to the fixtures. The force directions as well as gripping apparatus can be seen in Figure 3-33: Cross Tension Force Diagram and Figure 3-34: Instron Fixture for Cross Tension respectively.

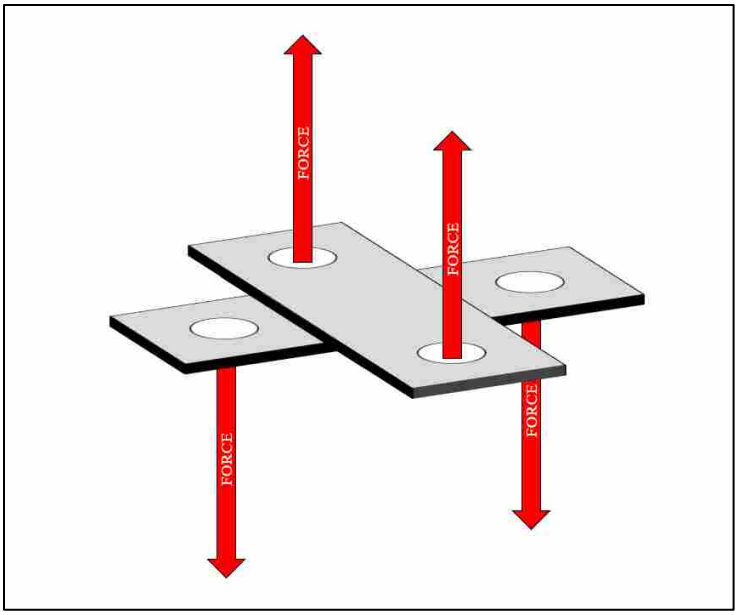

Figure 3-33: Cross Tension Force Diagram

Figure 3-34: Instron Fixture for Cross Tension

T-peel was configured using the Instron's jaws set to grab and pull the sample. No spacers were needed. The force directions as well as the gripping apparatus can be seen in Figure 3-35: T-Peel Force Diagram and Figure 3-32: Instron Jaws for Lap Shear and T-Peel respectively.

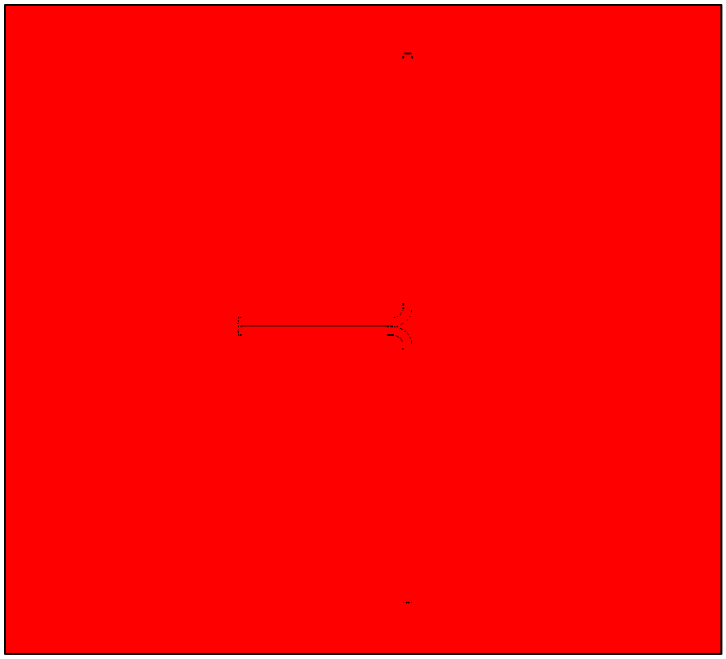

Figure 3-35: T-Peel Force Diagram

All data was recorded and collected on Instron machine other than failure mode which was recorded manually.

4 ANALYSIS

4.1 Introduction

The original intent of this research was to explore different application of FBJ. Specifically applications where an FBJ joint was formed joining two pieces of aluminum in which the consumable bit did not rely on one of the joining pieces to form the weld. This was accomplished through the use of a steel nut behind the aluminum to which the consumable bit could join. In this research we looked at two primary independent variables and conducted hypothesis testing on each. The independent variables were specifically number of flutes and shank diameter size. Graphs plotting peak weld strengths and independent variable settings were created and analyzed. Statistical significance was also calculated. Additionally, main effect and interaction was calculated for each of the data sets that were used in the 2^2 factorial design of experiement.

4.2 Welding Parameters

The objective and purpose of this research was to expand the scope of the FBJ technology. As such the focus was not on weld optimization. The initial welding parameters were set and maintained constant throughout all of the test samples. Hardness mapping of the weld site was done and can be seen in Figure 4-1: Hardness Map 1 for ECH10 and Figure 4-2: Hardness Map 2 for ECH10.

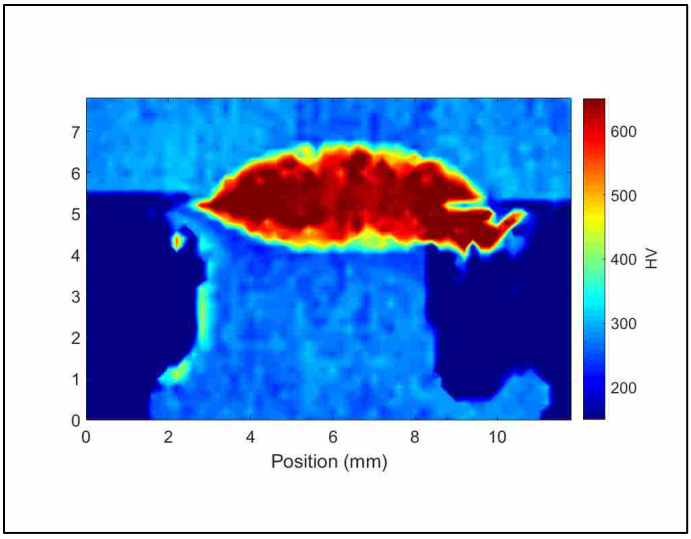

Figure 4-1: Hardness Map 1 for ECH10

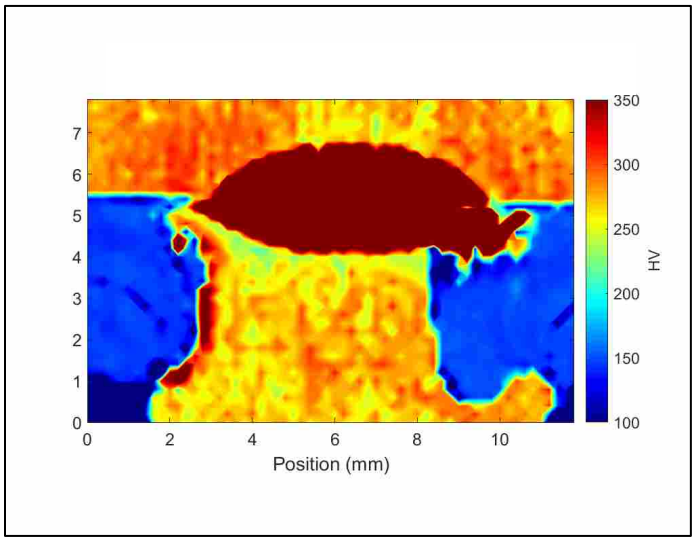

Figure 4-2: Hardness Map 2 for ECH10

Hardness mapping revealed an extremely hard heat affected zone (HAZ) as well as softening of the aluminum around the bit area. The high hardness indicates that the austenite was heated and cooled rapidly to form martensite. These results indicate what was targeted initially, a

sufficiently strong weld that would allow the study of the effect of flutes and shank diameter size.

It should be noted that Figure 4-2: Hardness Map 2 for ECH10, shows a slight, extremely thin line of hardening where the aluminum comes in contact with the bit. This is not a true hardening of the aluminum. Rather a limitation of the hardness testing tools used. The combination of the limitations of the resolution of the hardness testing equipment and visualization software created a false hardness assumption. The continuity of the hardness heat map is based on a non-continuous data points. This makes it necessary for the visualization software to assume a graduated scale in between data points. The line of hardened aluminum around the bit is simply an incorrect inference the visualization software made when transitioning form a relatively hard material to a relatively soft material.

4.3 Effects of Flute Quantity

The main purpose of flutes is to clear chips as the bit drills through the coupon material. Clearing chips is an important function in this variant of the FBJ process. Without the ability to clear chips, the bottom coupon material is pushed, instead of cut, out of the way. Because the two coupons are clamped together there is no predefined route for the material flow. As such, the material will follow the path of least resistance. In this case that pathway is up along the edge of the bit and out through the top coupon. As the bottom coupon material flows up the shank and out of the top coupon, the top coupon is displaced and deformed. The effect of this is a widening of the hole in the top aluminum coupon that the bit previously drilled. This means that there is less top coupon material sitting under the bit head. This leads to a weakening of the overall joint seen in premature HPT failures.

The purpose of varying flute quantity was to vary the amount of material cleared by the bit. By varying the amount of material cleared, the deformation to the top coupon was varied. The purpose of these experiments was to test how important top coupon deformation was to the strength of the final joint.

Data was collected on four bit variant types that investigated the effect of flute quantity on peak weld strength. The four bit types were:

1. ECHO6 – No flutes. Data was only collected for lap shear tests. See Figure 3-11: ECHO6 Bit.
2. ECHO9 – 2 flutes. Data was collected for lap shear, cross tension and t-peel tests. See Figure 3-12: ECHO9 Bit.
3. ECH10 – 3 flutes. Data was collected for lap shear, cross tension and t-peel tests. See Figure 3-13: ECH10 Bit
4. ECH12 – 3 flutes. Data was collected for lap shear, cross tension and t-peel tests. See Figure 3-15: ECH12 Bit. Note that ECH12 was designed to test for any interaction between the two independent variables and thus has a decreased shank size in addition to three flutes. Thus, results from this sample group may not be directly comparable to the other bit variants that are designed to test the effects of number of flutes on peak weld strength.

Average peak strength results from each of the tests can be viewed in Table 4-1: Average Peak Strength by Flute Quantity.

Average Peak Strength (STD) in Newtons				
Bit	Lap Shear	Cross Tension	T-Peel	Flutes
ECHO6	7892 (2020) N			0
ECHO9	10233 (345) N	3946 (495) N	2451 (294) N	2
ECH10	9778 (353) N	5777 (532) N	2605 (364) N	3
ECH12	7419 (1319) N	3741 (293) N	1721 (360) N	3

Table 4-1: Average Peak Strength by Flute Quantity

T-stat and corresponding P-Values were calculated for each of sample populations. T-stat and P-values can be viewed in Table 4-2: T-Stat and P-Value Tables for Varying Flute Quantities. P-values highlighted in green were found to be below a value of 0.05 signifying statistical significance. As each sample population is compared to each other to determine the effect of the change in independent variable, it is important to ensure that the sample populations are truly different. The T-stat and p-value tests confirmed whether or not sample populations were indeed different.

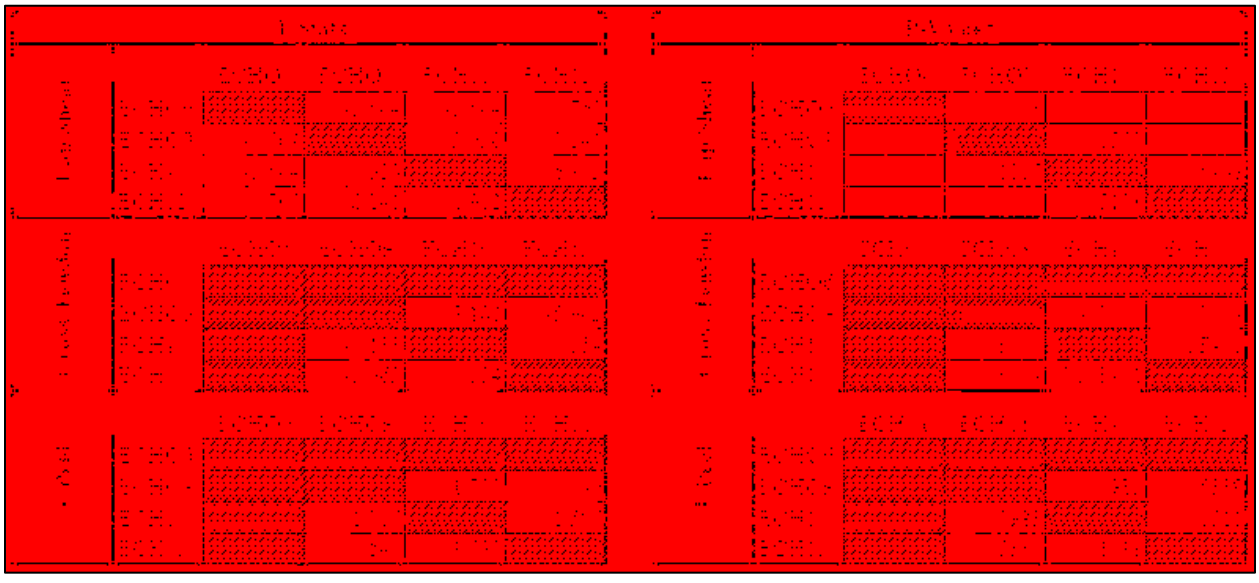

Table 4-2: T-Stat and P-Value Tables for Varying Flute Quantities

4.3.1 Effects of Quantity of Flutes in Lap Shear

In the lap shear test, the results prove that a statistically significant improvement in weld strength occurs when moving from zero to two flutes, however, no such empirical evidence is found when increasing the number of flutes beyond two as shown in Figure 4-3: Graph of Peak Strength for Lap Shear Tests.

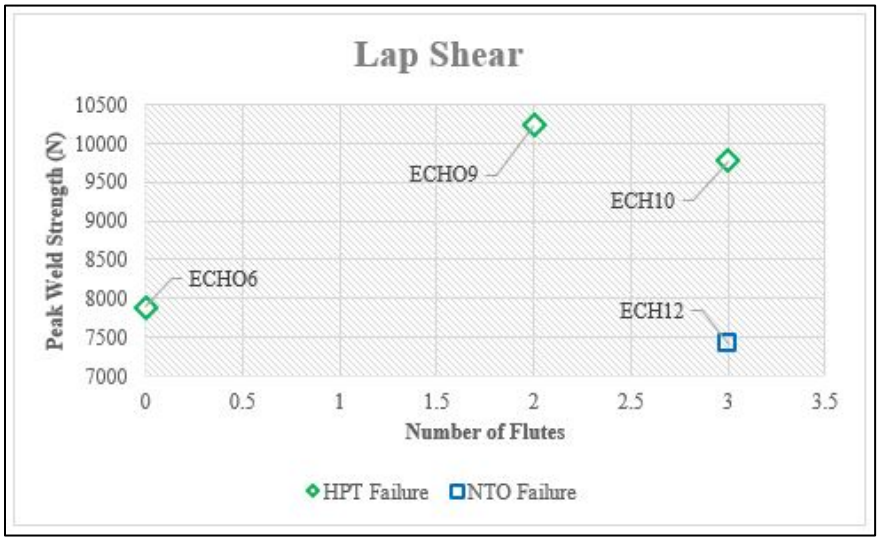

Figure 4-3: Graph of Peak Strength for Lap Shear Tests by Flutes

According to the data, flutes play an important role in increasing weld strength in the lap shear testing configuration. It does seem however, that there is a point of diminishing returns. Significant improvement was made moving from zero to two flutes, however, increasing beyond two flutes had no significant effect on weld strength. Bit design ECH10's peak strength does decrease slightly from measured results of ECHO9 in terms of averages, however no statistically significant difference was able to be detected between these sample groups. The cause for the discrepancy between ECH10 and ECH12 is attributed to the decreased shank diameter of ECH12 which was the only difference between the ECH10 and ECH12 test parameters.

Increasing flutes made a huge difference in the bits' ability to clear chips. This increased ability decreased the decreased top coupon deformation by better controlling bottom coupon material flow. Decreased top coupon deformation meant more material was left in place under the head of the bit, increasing the coupons ability to hold in place under load. This increased ability of the top coupon to stay in place under load can be clearly seen in the difference in peak weld strength between ECHO6 and ECHO9. The peak weld strengths for ECHO6 and ECHO9 were 7,892 N and 10,233 N respectively.

Going from two to three flutes had less of an effect. This is because a large step change was made in chip clearance when going from zero to two flutes, whereas a small incremental change was accomplished going from two to three flutes. Figure 4-4: ECHO9 and ECH10 Al Flow Comparison shows the difference, in Al coupon deformation between the ECHO9 and ECH10 joints. As can be observed, ECHO9 clearly has a significant amount of bottom coupon flow up the shaft and consequently, pushes the top coupon up and away from the optimal location of under the head of the bit. ECH10 does a better job of controlling flow and thus more of the top coupon is positioned under the bit head.

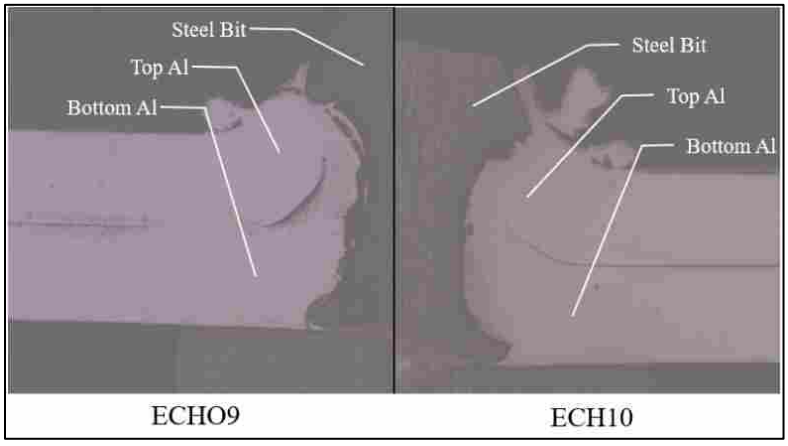

Figure 4-4: ECHO9 and ECH10 Al Flow Comparison

The reason why ECH10, despite having better bottom material flow control still had a lower average peak weld strength than ECHO9 can be explained by the testing method. The lap shear testing method, as seen in Figure 3-31: Lap Shear Force Diagram, places a horizontal load on the joint. In this horizontal load configuration, the strength created by the head and top coupon overlap is not the primary strength being tested. This strength only comes into play as the coupons and bit deform under load. The deformation leads to bending which is what puts the vertical load on the joint, see Figure 4-5: Lap Shear Bit Force Diagram. It is this vertical load that the bit head/coupon overlap resists. It is also this load that causes the joint to fail in the HPT failure mode.

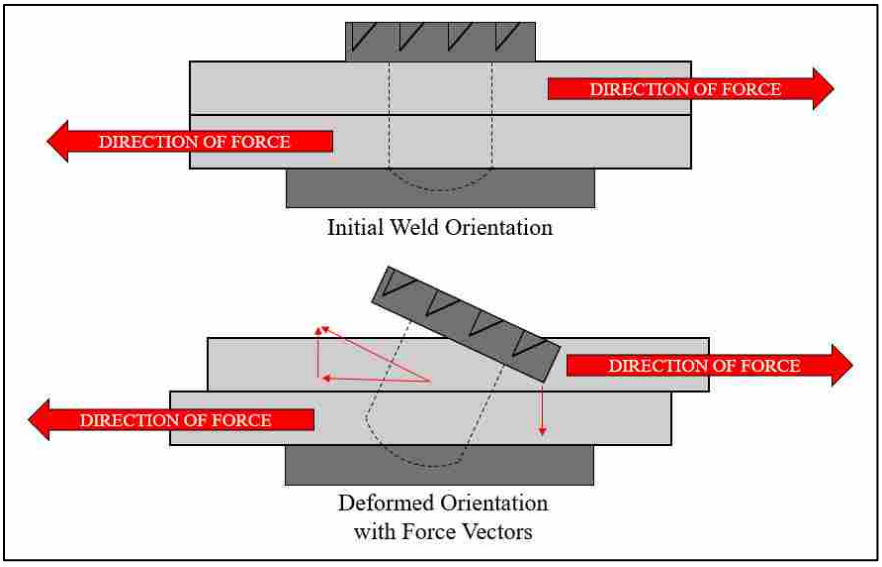

Figure 4-5: Lap Shear Bit Force Diagram

In lap shear testing the amount of coupon under the bit head is far less important than in other testing methods as the primary load is in the horizontal plane. As seen in Figure 4-4: ECHO9 and ECH10 Al Flow Comparison, the incremental difference made in bottom coupon material flow control ultimately doesn't do much in terms of adding strength to the joint. The

primary cause being the fact that bottom coupon material flow control is far less important in this testing method.

The addition of flutes also had a dramatic effect on increasing the repeatability of the tests. Material flow when left to itself to decide its own path was extremely inconsistent and was made manifest in the STD of ECHO6. When controlled, material flow becomes extremely more predictable as was seen in the ECHO9 sample group STD. The STD of ECHO6 was 2,020 N whereas the STD for the ECHO9 sample group was 345 N. The large STD of ECHO6 is the reason why ECHO6 was not used as a baseline sample.

4.3.2 Effects of Flute Quantity in Cross Tension

It is understood that there is not a single universal set of parameters that will optimize results for the lap shear, cross tension and t-peel tests for the FBJ method (Shirley, 2018). The results for cross tension were consistent with this understanding as seen in Figure 4-6: Graph of Peak Strength for Cross Tension Tests.

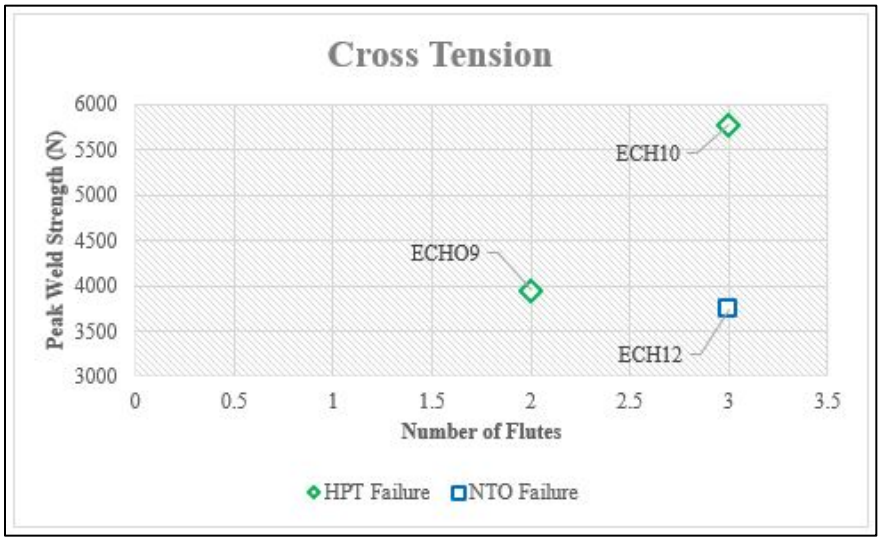

Figure 4-6: Graph of Peak Strength for Cross Tension Tests by Flutes

A statistically significant difference was observed between the ECHO9 and ECH10 tests increasing weld strength by over 1,800 N. Once again, there was a significant difference between ECHO9 and ECH12 tests, however in addition to additional flutes, ECH12 has a decreased shank diameter. The statistically significant discrepancy between ECH10 and ECH12 being attributed to the decreased shank diameter. Supporting this is the observation that failure mode switched between ECH10 and ECH12, from HPT to NTO respectively. This signifies that the switch in failure mode was due to something other than number of flutes.

The ECH10 sample group was found to perform significantly better in cross tension than did ECHO9. This is different than what we observed in lap shear. Figure 4-4: ECHO9 and ECH10 Al Flow Comparison shows an improvement in bottom coupon material flow control with the addition of a single flute to the bit design. In lap shear this incremental improvement in flow control made no difference in results as the lap shear test configuration loads the joint in the horizonal plane. In the cross tension testing configuration, loads are configured in the vertical plane, as seen in Figure 4-7: Cross Tension Bit Force Diagram, making the top coupon/head overlap critical.

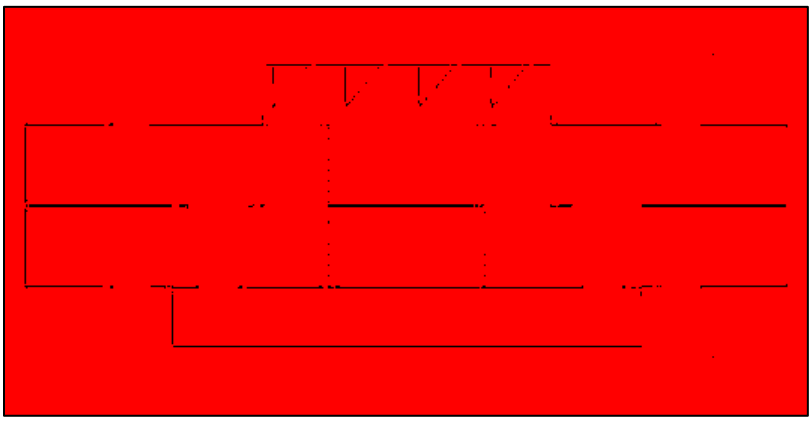

Figure 4-7: Cross Tension Bit Force Diagram

The small improvement in bottom coupon material flow control made a large difference in overall peak weld strengths. ECHO9 measured 3,946 N while ECH10 measured 5,777 N. Decreasing top coupon deformation left more of the top coupon positioned under the head of the bit which is what accounted for increased strength in the Z direction.

4.3.3 Effects of Flute Quantity in T-Peel

T-peel tests show a similar result as obtained in the lap shear tests. There was slight movement in averages going from two to three flutes as seen in Figure 4-8: Graph of Peak Strength for T-Peel Tests.

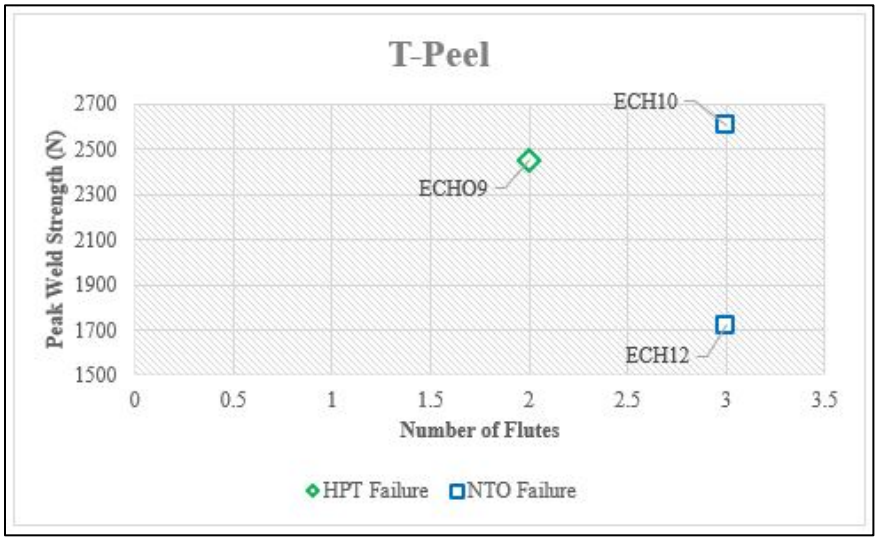

Figure 4-8: Graph of Peak Strength for T-Peel Tests by Flutes

Unfortunately no statistical significance was observed between any of the sample groups. Bit design ECHO6 was not tested in the t-peel configuration so it is impossible to say definitively what effect going from zero to two flutes has on this test. Additionally, ECH10's failure mode was different than ECHO9's so it is impossible to get an idea of the magnitude of

strength increase that an additional flute provided. As seen in other sample groups, ECH12 was significantly lower in peak weld strength than the other samples. The cause for this is attributed to decreased shank size as was discussed in earlier sections.

It is important to note that the observed method of failure changed between ECHO9 and ECH10 sample groups. ECHO9's primary failure mode was HPT while ECH10's primary failure mode was NTO. The consistency of the failure mode was strong as well. ECHO9 failed 100% of the time in HPT mode and ECH10 failed 100% of the time in NPT mode. This observation provides supporting evidence that an additional flute and increased material flow control contributed to the joint strength. Because the failure mode changed we know that either the additional flute increased the strength of the joint specifically in the bit head region or that the decreased surface area with the additional flute decreased the bit-nut sections strength. Since overall strength did not go down, but in fact actually increased in terms of averages, it is reasonable to assume that the increased material flow control contributed strength to the head region rather than the decreased surface area reduced strength in the bit-nut region. This assumption supports the finding that increasing number of flutes benefits peak weld strength in the t-peel testing configuration.

4.3.4 Summary of Effects of Flute Quantity

The research indicates that the quantity of flutes plays an important role in peak weld strength. It is acknowledged, however, that the effect of flute quantity varies depending on test method. Flute quantity was found to be effective to a point in the lap shear testing configuration while being extremely important in cross tension and important in t-peel. In lap shear, adding up to two flutes had a profound effect on peak weld strength while in cross tension and t-peel, up to

three flutes were found to produce significant results. These results were obtained through improved bottom coupon material flow control. The improved material evacuation through increased flutes led to less top coupon deformation. This decreased deformation resulted in more material from the top coupon under the bit head adding strength to the bit head region of the joint. This in many cases improved the overall joint strength. As seen in Figure 4-4: ECHO9 and ECH10 Al Flow Comparison, even in this research's best samples, deformation of the top coupon still occurred. Improving the drilling process through varied flute size, hardened bit tips or other methods would, theoretically, increase joint strength even more.

4.4 Effects of Shank Diameter

The diameter of the shank determines the amount of overhang the bit head creates. In this set of experiments the amount of overhang and how it affects peak weld strength was studied. Varying the amount of overhang affected the amount of material of the top coupon located under the head. The theory was that the lower the ratio between bit shank diameter and bit head diameter (ie, amount of overhang) the stronger the joint would be. This experiment was similar to the experiments with flute quantity however, rather than looking at decreasing top coupon deformation this grouping of tests looked specifically at bit head overhang.

Data was collected on three bit designs that tested the effect of bit diameter on peak weld strength. The three bit designs that were tested were:

1. ECHO9 – diameter was 0.280". See Figure 3-12: ECHO9 Bit.
2. ECH13 – diameter was 0.250". See Figure 3-16: ECH13 Bit.
3. ECH11 – diameter was 0.220". See Figure 3-14: ECH11 Bit.

Average peak strengths for each bit design can be found in Table 4-3: Average Peak Strength by Varying Bit Diameter.

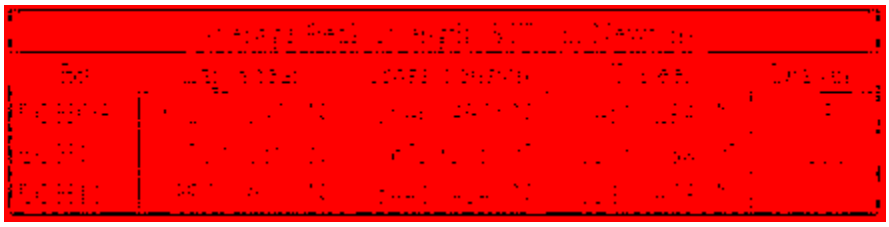

Table 4-3: Average Peak Strength by Varying Bit Diameter

T-stat and corresponding P-Values were calculated for each of the sample populations. T-stat and P-values can be viewed in Table 4-4: T-Stat and P-Value Tables by Varying Bit Diameters. P-values highlighted in green were found to be below a value of 0.05 signifying statistical significance.

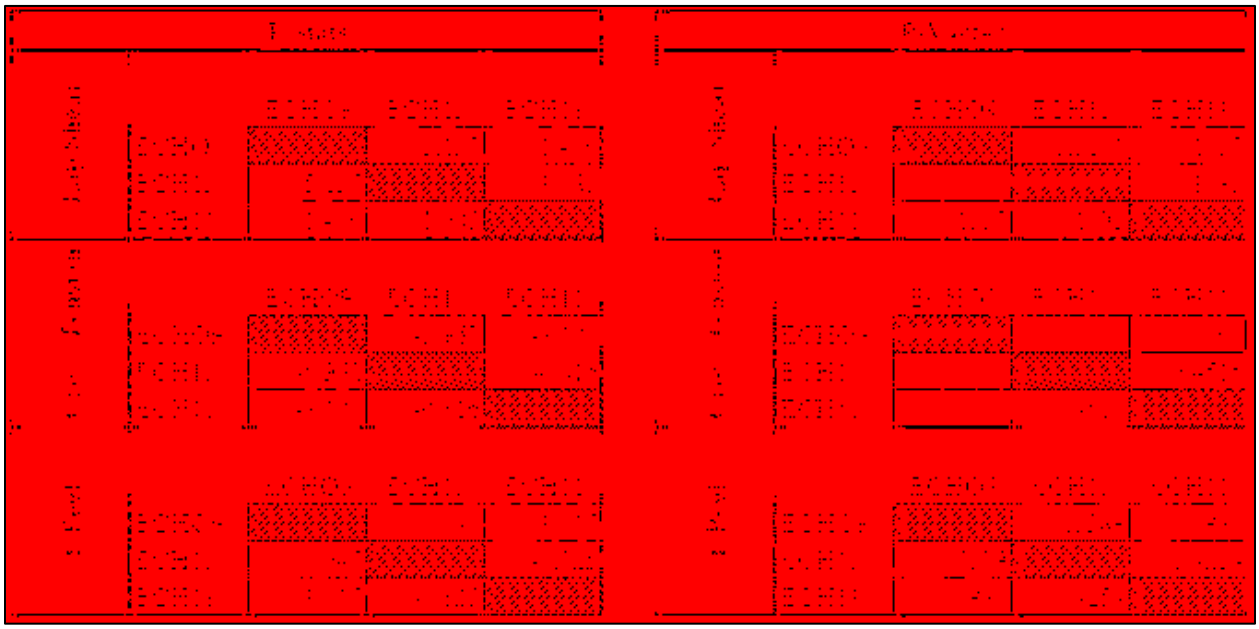

Table 4-4: T-Stat and P-Value Tables by Varying Bit Diameters

4.4.1 Effects of Shank Diameter on Lap Shear

Lap shear tests indicate that, as found in other research, no global parameter set exists for optimization across all tests as seen in Figure 4-9: Graph of Peak Strength for Lap Shear Tests.

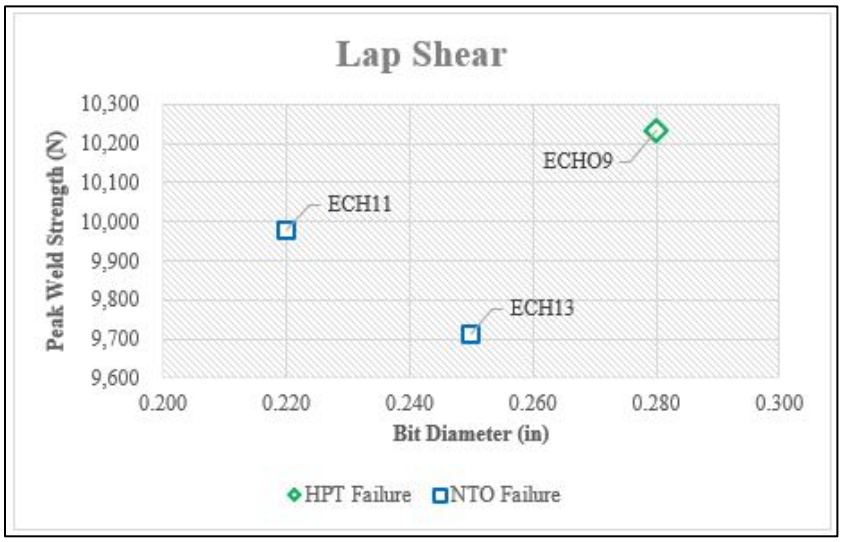

Figure 4-9: Graph of Peak Strength for Lap Shear Tests by Diameter

Statistically significant differences were observed between the ECHO9 and ECH13 sample groups, however ECH11 could not be determined to be different from either the ECHO9 or ECH13 groups in any statistically significant way as seen in Table 4-4: T-Stat and P-Value Tables by Varying Bit Diameters.

An important observational result obtained was that the failure mode was different for ECH13 and ECH11 than it was for ECHO9. All of the samples from the ECH13 group failed in the NTO mode, whereas 67% of the failures in the ECHO9 group were categorized as HPT failures, the remaining 33% being NTO. As the weld strength has yet to approach the tear strength of the aluminum coupons or the shear strength of the steel bit at these diameters, a hypothetically 50-50 split between NTO failures and HPT failures should result as the optimized

shank diameter is approached. Results from the ECHO9 and ECH13 groupings support this theory. ECHO9 was significantly stronger than ECH13 and had a failure ratio closer to the 50-50 split we would see on a fully optimized bit diameter. Thus it is believed that the true optimized location lies somewhere between the bit diameters of ECH13 and ECHO9.

A closer inspection of the joint revealed that the decreased shank size did indeed increase the amount of overlap between the top coupon and the bit head. As seen in Figure 4-10: ECHO9 and ECH11 Al Flow Comparison top coupon and bit overlap is significantly better in ECH11 than ECHO9. The decreased shank size of ECH11 contributed in multiple ways to the improved overlap. Although there were only two flutes in the ECH11 bit, the decreased shank size meant that the amount of material that needed to be removed was significantly less which improved the efficiency of the flutes. This had the same effect as increasing number of flutes as it decreased bottom coupon material flow thereby decreasing top coupon deformation. Additionally the broader head diameter to shank diameter ratio provided more area for the top coupon to nest under. Both of these factors contributed to significantly more material under the bit head than seen in other bit designs.

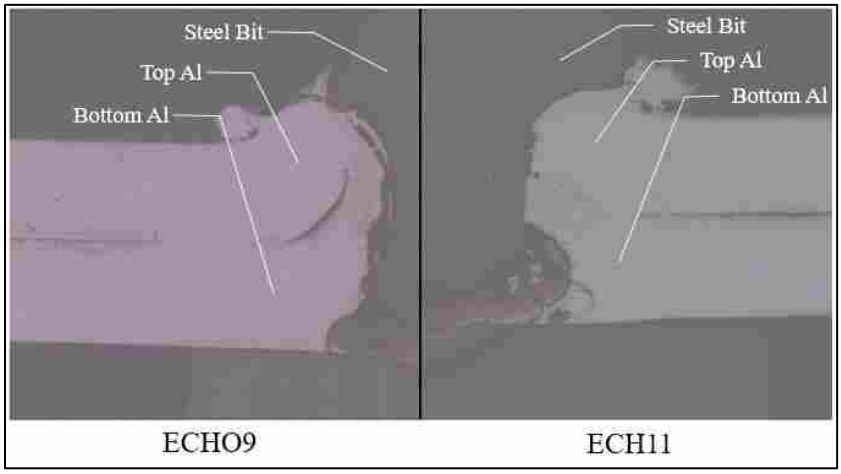

Figure 4-10: ECHO9 and ECH11 Al Flow Comparison

While bit head and coupon overlap was significantly improved in ECH11 over ECHO9, the overall strength decreased, albeit not in a statistically significant way. The overall decrease in strength can be explained by the decreased surface area in the bit-nut region. Because the bit shank diameter was downsized, a corresponding reduction in surface area followed. This reduction in surface area where the weld was formed decreased the strength of that area of the joint leading to premature failure. This explanation is further supported by the fact that the failure mode changed between the ECHO9 and ECH11 test from HPT to NTO respectively. This shift signifies a weakening in the bit-nut area of the joint.

While we cannot empirically prove though this grouping of data that decreased shank size improved weld strength, the results and learnings obtained through the flute quantity experiments indicate that decreased shank diameter should improve joint strength in the bit head region. It was found that improving chip clearance and thereby improving top coupon deformation, effectively increases bit head and coupon overlap. This has proven to be successful at improving joint strength in the bit head region of the joint.

As with most optimizations there is a tradeoff. In the case of bit shank size diameter the tradeoff is either increased overlap or increased bit-nut weld strength. In the case of ECH11 it seems that the shank size was decreased too much thereby weakening the bit-nut joint which translated into and overall decrease in joint strength.

4.4.2 Effects of Shank Diameter on Cross Tension

In the cross tension test, results indicate a single maximum in terms of peak weld strength and bit diameter as shown in Figure 4-11: Graph of Peak Strength for Cross Tension Tests.

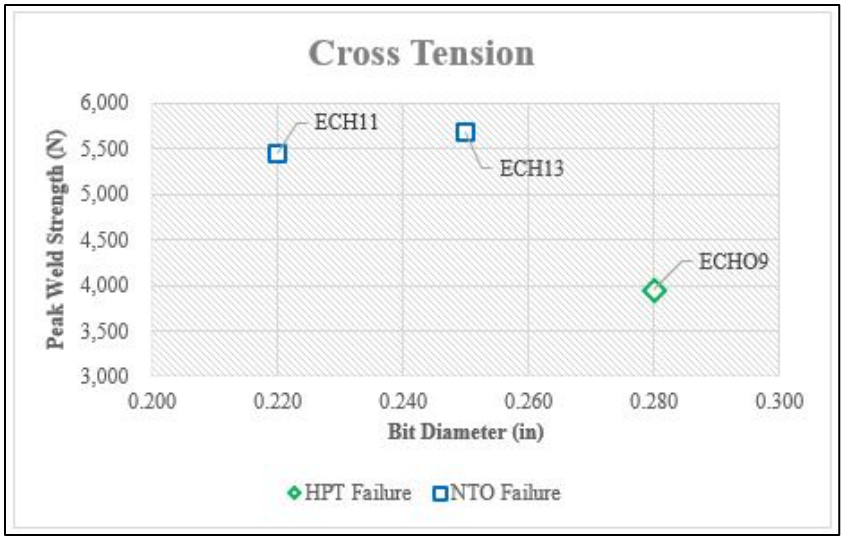

Figure 4-11: Graph of Peak Strength for Cross Tension Tests by Diameter

Statistical significance was calculated between the ECHO9 and both the ECH11 and ECH13 sample groups. Statistical significance could not be determined for the ECH11 and ECH13 sample groups. The results infer that a global maximum exists.

Joint strength was increased by decreasing the bit diameter as is seen in the peak strength results in Table 4-3: Average Peak Strength by Varying Bit Diameter. As was observed in Figure 4-10: ECHO9 and ECH11 Al Flow Comparison, there was a significantly better head to coupon overlap in ECH11 than ECHO9. The broadened head to shank ratio of ECH11 was responsible for the improved head to coupon overlap. This increased overlap added strength to the bit head region which is why a change in failure mode and increase in overall joint strength was observed in ECH11 and ECH13 in comparison with ECHO9.

Both ECHO9 and ECH13 had a 100% HPT and NTO failures respectively, while ECH11 had 87.5% NTO failures the other 12.5% being HPT. While on the surface these results do not seem to provide support for the theory that as the optimized shank diameter is approached a 50-

50 split between NTO and HPT failures will be observed, it is important to take into consideration sample size. Both the ECHO9 and ECH1 sample groups consist of sixteen samples while the ECH13 group consists of only 5 samples. It is believed that had more samples been run in the ECH13 configuration more HPT failures would have been observed.

These findings are also consistent with the flute quantity findings. As was discussed earlier with Figure 4-7: Cross Tension Bit Force Diagram, top coupon deformation and bit head overlap are significantly more important in determining joint strength in cross tension testing than lap shear testing. Improving bit-nut strength through optimized weld settings or other methods should increase the overall strength of the joint beyond the results that were obtained in this research.

4.4.3 Effects of Shank Diameter on T-Peel

As in cross tension, t-peel tests also seemed to indicate a broader head to coupon overlap as being advantageous as seen in Figure 4-12: Graph of Peak Strength for T-Peel Tests.

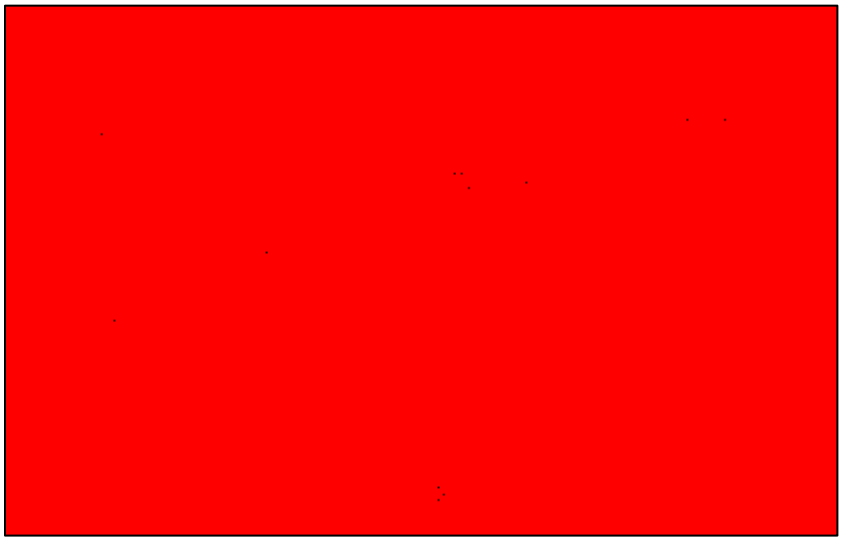

Figure 4-12: Graph of Peak Strength for T-Peel Tests by Diameter

As with the investigation of number of flutes vs peak weld strength, T-peel sample date proved to be statistically insignificant. The ECHO9 failure mode was different than the failure mode of ECH11 or ECH13 and offers a clearer understanding of what went on in this sample group. All three sample groups failed 100% of the time in their respective modes. The data shows that the change in bit diameter had an effect of changing the failure mode from NTO at the smaller diameters, to HPT at the larger diameters. This result can be explained by two contributing factors. First increased head to coupon overlap and decreased surface area of the weld. In the case of comparing ECHO9 with ECH11 and ECH13, it seems that both the ECH11 and ECH13 diameters were decreased too far, sacrificing too much strength at the nut. This imbalance led to an overall decrease in joint strength. Improvements to overall joint strength could be made by reducing bit diameter size from that of ECHO9.

4.4.4 Summary of Effects of Shank Diameter

As was the case in the flute quantity investigation, shank diameter is another important factor in overall joint weld strength. Optimal diameter varied by each testing case. An important finding was the tradeoff between head-coupon overlap and surface area. This tradeoff affected the overall joint strength by trading strength between the bit head region and the bit-nut region of the joint. Decreasing the shank diameter has been observed to increase the joint strength in the region of the bit head while simultaneously decreasing the bit-nut localized strength of the joint. Shank diameter was found to be a useful lever in balancing the strengths of the two localized joint regions. It very effective at changing the failure mode from HPT to NTO or vice versa. This is an important finding as optimization work continues on the FBJ project. If, for example, improvements are made on the weld joint through optimized parameters or materials, strength can be transferred to the head via changing the shank diameter.

4.5 Effects of Surface Area

The DOE was originally designed to test two separate independent variables. The first being number of flutes and the second being bit diameter size. Originally the experiments were thought to be exclusive with the exception of ECH12 which was designed to test any possible interaction between the two independent variables. As results began to be collected a third criteria was introduced against which the results could be measured. Bit surface area was found to be a useful measure against which a comparison could be made to peak weld strength. Surface Area equations for each of the bit designs can be found in Appendix B – Surface Area Calculations and Equation.

4.5.1 Effects of Surface Area on Lap Shear

When plotted against surface area, lap shear results had a convex shape providing evidence for a potential global maximum as seen in Figure 4-13: Graph of Peak Strength for Lap Shear .

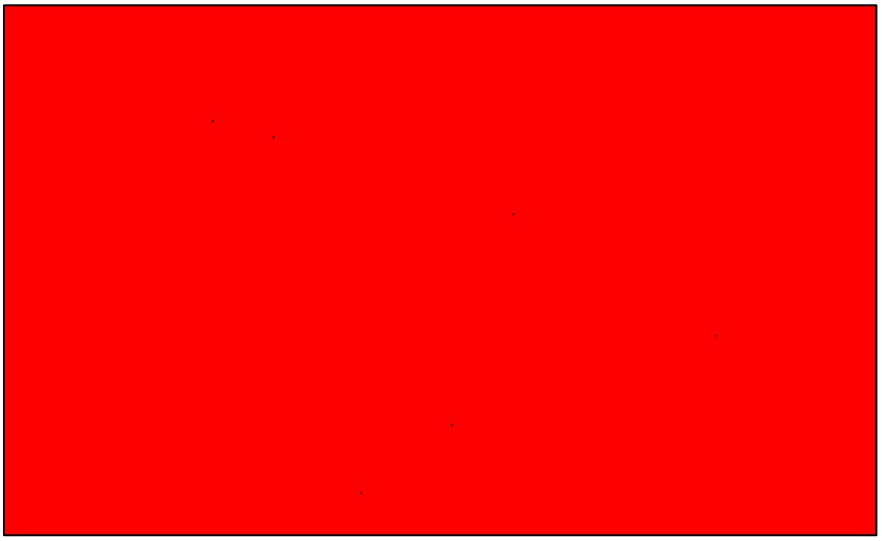

Figure 4-13: Graph of Peak Strength for Lap Shear by Surface Area

A polynomial trendline of the second order was fitted to the plotted data. The R^2 of the trendline was very good at 0.78. The equation for the trend line in Figure 4-13: Graph of Peak Strength for Lap Shear was found to be:

$$y = -6002312x^2 + 505049x - 471 \quad (4\text{-}1)$$

Using this equation the apex of the trendline was calculated to be 10,153 N. The hypothetical optimal surface area was 0.042 in^2. The graphed trendline is right in line with our results. The high R^2 for the inverted second degree polynomial signify that there is indeed an inflection point indicating the presence of maximum. This supports the original hypothesis that there is an optimal bit diameter to head diameter ratio as it relates to weld strength.

The apex of the curve sits approximately where the failure modes transition from NTO to HPT. ECH10 is on the wrong side of the curve, however, ECH10's main failure mode, HPT, only occurred 68.8% of the time. The other 31.2% of the time ECH10 failed in NTO mode. This indicates that the ECH10 tests were close to the optimal point as the ECH10 failure ratio approached a 50-50 split. Additionally variation exists in the sample data and the curve fit is not perfect.

One important observation as it relates to Figure 4-13: Graph of Peak Strength for Lap Shear , is how the failure type changes as bit surface area increases. As bit surface area increases, the failure type changes from NTO to HPT. Increased surface area means increased contact area between the bit and nut. This translates into a larger weld as seen in Figure 4-14: ECHO9 and ECH12 Weld Site Comparison. ECHO9 has a surface area of 0.0616 in^2 whereas ECH12 has the smallest surface area of 0.0230 in^2. The difference in the size of weld nugget is considerable.

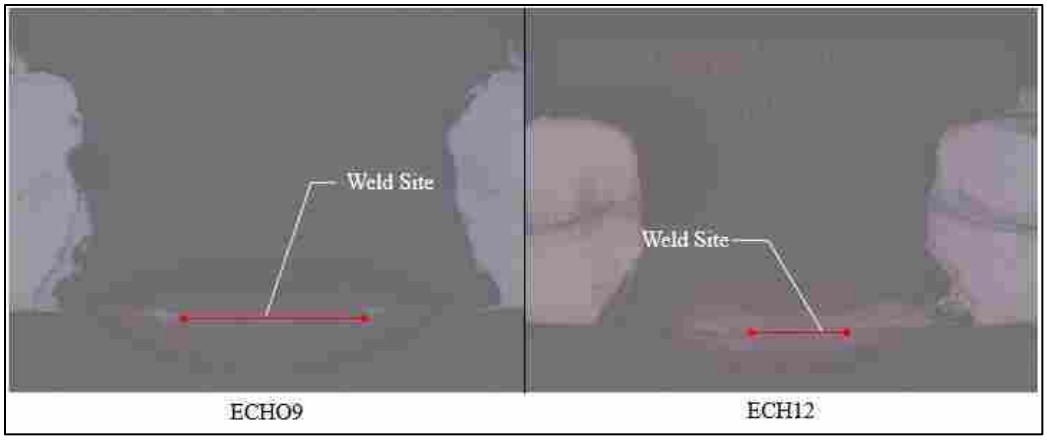

Figure 4-14: ECHO9 and ECH12 Weld Site Comparison

The decreasing weld nugget size and increasing head-coupon overlap as the diameter shrinks is what drives the change in failure mode as the surface area either grows or shrinks.

4.5.2 Effects of Surface Area on Cross Tension

Cross tension results were plotted and the results showed a convex curve with a maximum apex as seen in Figure 4-15: Graph of Peak Strength for Cross Tension .

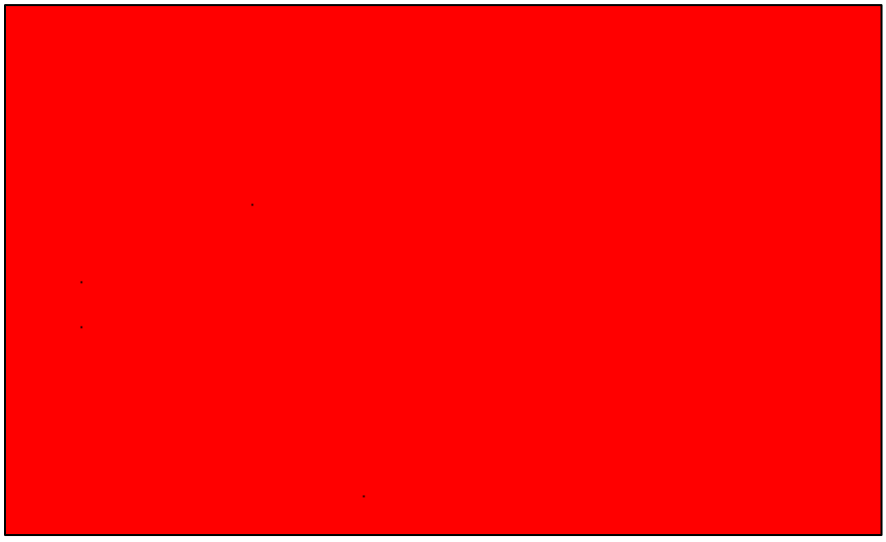

Figure 4-15: Graph of Peak Strength for Cross Tension by Surface Area

A polynomial trendline of the second order was fitted to the plotted data. The R^2 of the trendline was excellent at 0.99. The equation for the trend line in Figure 4-15: Graph of Peak Strength for Cross Tension was found to be:

$$y = -16022754x^2 + 1111471x - 13275 \quad (4\text{-}2)$$

Using this equation the apex of the trendline and optimal peak weld strength was calculated to be 6000 N. The hypothetical optimal surface area was 0.035 in^2. The extremely high R^2 of the trendline indicates a good fit and positive evidence for an inverted convex shape. This supports the hypothesis that there exists an optimal ratio between surface area and head diameter that results in a higher peak weld strength.

Again, it should be noted that sample group ECH13 is on the wrong side of the inflection point. While ECH13's failure mode was extremely consistent, ECH13 sample size was only five tests. Additionally statistics could not conclude there was a significant difference between the sample groups ECH10, ECH11, and ECH13. Thus there is some uncertainty about where the true means lie in relation to one another. There can be, however, a great deal of confidence in the shape of trendline as there was a statistically significant difference between the lower data points, ECHO9 and ECH12, and the upper data points, ECH10, ECH11 and ECH13.

The same phenomenon was observed in cross tension as was in lap shear. That being that the failure mode seemed to switch from NTO to HPT as the surface area grew in relation to the head diameter. This phenomenon was caused by the same tradeoff between weld nugget size and head-coupon overlap discussed in the lap shear section and seen in Figure 4-14: ECHO9 and ECH12 Weld Site Comparison.

4.5.3 Effects of Surface Area on T-Peel

T-peel results were plotted similarly to the results from the lap shear and cross tension tests. The results showed a slightly less steep convex curve with a maximum apex as seen in Figure 4-15: Graph of Peak Strength for Cross Tension .

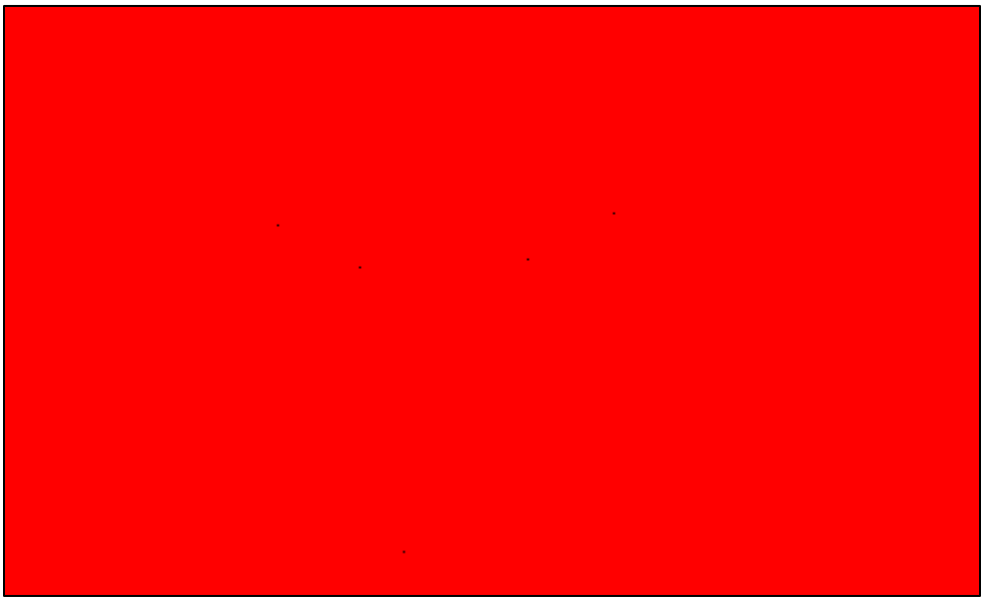

Figure 4-16: Graph of Peak Strength for T-Peel by Surface Area

A polynomial trendline of the second order was fitted to the plotted data. The R^2 of the trendline was very good at 0.91. The equation for the trendline in Figure 4-16: Graph of Peak Strength for T-Peel was found to be:

$$y = -2546633x\text{^}2 + 205098x - 1612 \quad (4\text{-}3)$$

Using this equation the apex of the trendline and optimal peak weld strength was calculated to be 2517 N. The hypothetical optimal surface area was 0.040 in^2. The high R^2 of the

trendline indicates a good fit and positive evidence for an inverted convex shape. This supports the hypothesis that there exists an optimal ratio between surface area and head diameter that results in a higher peak weld strength. T-peel evidence is the weakest of the three tests. Few statistically significant relationships were found. This is shown as we see that the only statistically significant difference detected for ECHO9 was with ECH12. Additionally ECH13 was also not found to be statistically significant with any of the other sample groups excluding ECH12. The lack of statistical significance sheds some doubt on the reliability of the results, however, when taken in whole, reasonable confidence can be had in regards to the shape of trendline.

4.5.4 Summary of Effects of Surface Area

Surface area was found to be an important measure as it relates to NTO failures. It was found that the smaller the surface area the weaker the weld at the bit-nut interface. It should be recognized that there are many different avenues that could be explored to improve the weld at the bit-nut interface from the testing parameters used in this research. Improved material selection and optimized welding parameters are provided as a few examples. Doing so would increase the strength of the bit-nut joint area and allow for the shank size to be decreased transferring strength to the bit head area of the joint via a larger head-coupon overlap.

4.6 Interaction of Flute Quantity and Shank Diameter

A 2^2 factorial experiment was conducted to examine the interactions between shank diameter and flute quantity. The X_1 varible was the shank diameter with a two values with either a high (0.280 in) or low (0.220 in) setting. The X_2 variable was the quantity of flutes which also

had two values, both a high (3 flutes) and a low (2 flutes) setting as outlined in Figure 4-17: DOE Setup Structure.

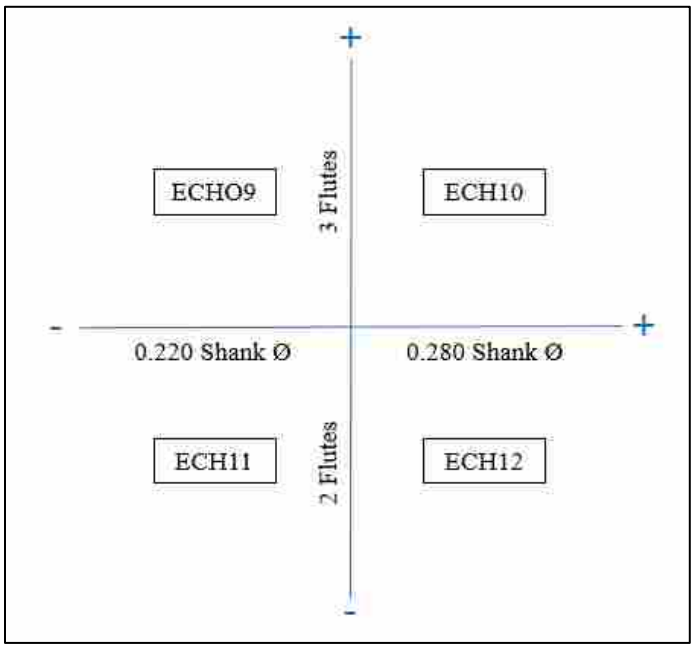

Figure 4-17: DOE Setup Structure

4.6.1 Lap Shear DOE Findings

The main effect values for both the X_1 and X_2 variables were calculated. A summary of the main effects can be found in Table 4-5: Summary of Lap Shear Main Effects.

Lap Shear	Main Effect X1 (Low X2)	256.19
	Main Effect X1 (High X2)	2,358.88
	Main Effect X2 (Low X1)	(2,557.88)
	Main Effect X2 (High X1)	(455.19)
	Average Main Effect X1	1,307.53
	Average Main Effect X2	(1,506.53)

Table 4-5: Summary of Lap Shear Main Effects

Main effects for lap shear suggest that increasing shank diameter size has an overall positive effect regardless of if quantity of flutes is in its high (three) or low (two) states. While increasing diameter size was shown to be a positive regardless of the situation, a substantially greater effect was observed when flute quantity was at its high state of three flutes. Additionally, opposite the shank diameter findings, additional flutes had a negative effect at both high and low shank diameter settings with the more pronounced effect when shank diameter was at its lower setting. T-tests were conducted for the average main effect of both the X_1 and X_2 variables. T scores of 6.95 and -8.01 were calculated respectively. When compared with the 2.001 t statistic at a probability of 0.05 the average main effects were both found to be statistically significant.

Interactions for the 2^2 factorial design were calculated for the lap shear testing configuration and found to be 1051 N. Additionally a t score of 5.59 was calculated for the interaction providing evidence of statistical significance when compared with the t statistic of 2.78.

4.6.2 Cross Tension DOE Findings

The main effect values for both the X_1 and X_2 variables were calculated. A summary of the main effects can be found in Table 4-6: Summary of Cross Tension Main Effects.

Cross Tension	Main Effect X1 (Low X2)	(1,495.63)
	Main Effect X1 (High X2)	2,035.66
	Main Effect X2 (Low X1)	(1,700.44)
	Main Effect X2 (High X1)	1,830.85
	Average Main Effect X1	270.02
	Average Main Effect X2	65.20

Table 4-6: Summary of Cross Tension Main Effects

Main effects for cross tension differ from those of lap shear. In the cross tension experiment, it was found that overall both the X_1 and X_2 variables had overall positive main effects. It should be noted however that both variables had negative effects when the other variable was at its low levels. This suggests that increasing shank size and flute quantity is only beneficial when the other variable is has already been increased to its high state. Otherwise the increase of one variable will have a negative effect. T-tests were conducted for the average main effect of both the X_1 and X_2 variables. T scores of 2.37 and 0.57 were calculated respectively. When compared with the 2.0003 t statistic at a probability of 0.05 the average main effects of X_1 (shank size) were found to be statistically significant while the main effects of X_2 (flute quantity) were not.

Interactions for the 2^2 factorial design were calculated for the cross tension testing configuration and found to be 1766 N. Additionally a t score of 4.17 was calculated for the interaction providing evidence of statistical significance when compared with the t statistic of 2.78.

4.6.3 T-Peel DOE Findings

The main effect values for both the X_1 and X_2 variables were calculated. A summary of the main effects can be found in Table 4-7: Summary of T-Peel Main Effects.

T-Peel	Main Effect X1 (Low X2)	241.06
	Main Effect X1 (High X2)	884.69
	Main Effect X2 (Low X1)	(489.00)
	Main Effect X2 (High X1)	154.63
	Average Main Effect X1	562.88
	Average Main Effect X2	(167.19)

Table 4-7: Summary of T-Peel Main Effects

Main effects for t-peel were most similar to those of lap shear. Shank diameter had an overall positive effect while flute quantity had an overall slightly negative effect. In the case of shank diameter at all levels it proved to be a good thing to increase shank diameter. In the case of flute quantity it was positive increasing flute quantity at the higher diameter, but detrimental increasing flute quantity at the lower levels. T-tests were conducted for the average main effect of both the X_1 and X_2 variables. T scores of 6.01 and -1.78 were calculated respectively. When compared with the 2.000 t stat at a probability of 0.05 the average main effects of X_1 (shank size) were found to be statistically significant while the main effects of X_2 (flute quantity) was not.

Interactions for the 2^2 factorial design were calculated for the cross tension testing configuration and found to be 321 N. A t score of 0.13 was calculated for the interaction providing no evidence of statistical significance when compared with the t stat of 2.78.

4.6.4 Summary of DOE Findings

The main effect findings of both shank diameter at the high level of flutes quantity as well as flute quantity at the lower level of shank diameter were consistent across all test cases, lap shear, cross tension and t-peel. It was found that the larger shank diameter had a positive effect when flute quantity was three. Additionally it was found that three flutes was detrimental at the smaller diameter. This analysis is right in line with the surface area findings outlined in the Effects of Surface Area section.as surface area of the bit tip is decreased with more flutes, it is beneficial to have a large overall diameter to offset some of the lost surface area due to additional flutes. Additionally as shank diameter decreased, adding additional flutes, reduces weld surface area further compounding the reduced area.

The main effect of increasing shank diameter in samples with two flutes proved to be minimally impactful in lap shear and t-peel testing, however was extremely important in cross

tension testing. Cross tension results showed an large negative effect for higher bit diameters at the two flute setting. This is also in line with the findings of this research as drilling seems to be the most critical in the cross tension tests. Figure 4-10: ECHO9 and ECH11 Al Flow Comparison show the flow path of the aluminum from the bottom coupon. Aluminum not cleared by the flutes pushes its way upward through the top coupon, widening the hole around the bit. This effectively leaves less top coupon material under the bit weakening the holding strength of the bit head. The vertical load that cross tension testing places on the joint, as seen in Figure 4-7: Cross Tension Bit Force Diagram, amplifies this type of process deficiency. Lap shear and t-peel testing place a partial horizontal load on the joint, as seen in Figure 4-5: Lap Shear Bit Force Diagram and Figure 4-7: Cross Tension Bit Force Diagram respectively. This horizontal load detracts from the vertical load and the joint is less affected by the loss of material under the nut head.

The main effect of going from two to three flutes on large diameter bits was seen to be positive for all tests with the exception of lap shear. It was found to be very beneficial for cross tension while being only mildly beneficial for t-peel. Again, because of the pure vertical load placed on the join in cross tension testing drilling is an extremely important function. It follows that increasing quantity of flutes would aid drilling and material removal which in turn would have a positive effect on peak weld strength.

4.7 FBJ Comparison with Other Joining Processes

4.7.1 FBJ Comparison to Resistance Spot Welding

RSW joint results were found for joining aluminum with aluminum and are summarized in Table 2-1: Summary of RSW Results In short Sun et al. tested joining two pieces of aluminum

of the same thickness using the RSW process. Sun et al had a large sample size and extremely consistent results. The FBJ process here stacks up well to RSW process. A comparison of results can be seen in Table 4-8: Comparison of RSW and FBJ Results.

Table 4-8: Comparison of RSW and FBJ Results

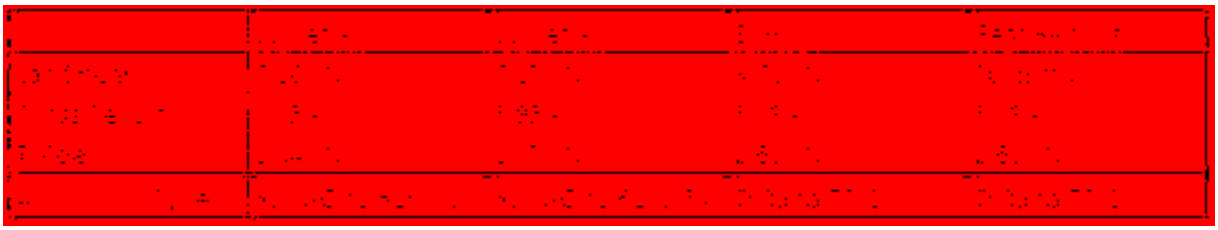

As can be seen, FBJ was superior in all tests with the exception of cross tension. T-peel and lap shear results were significantly higher, exceeding RSW results by 1.24 kN and 2.61 kN respectively. FBJ cross tension was lower, however, only by 0.27 kN. Advantages to FBJ include the superior strength achievable in addition to the low power consumption in comparison to RSW. Disadvantages to FBJ include the increased deformation of the working material compared to RSW as well as the use of a consumable bit to join products.

4.7.2 FBJ Comparison to Clinching

Clinched joints were formed using two pieces of aluminum, AL6061 and AL5052 by Chen. Unfortunately clinched joints using two pieces of aluminum were only tested in the lap shear and cross tension configurations. Data could not be found on clinched t- peel joints using only aluminum. The comparison results can be seen in Table 4-9: Comparison of Clinching and FBJ Results

Table 4-9: Comparison of Clinching and FBJ Results

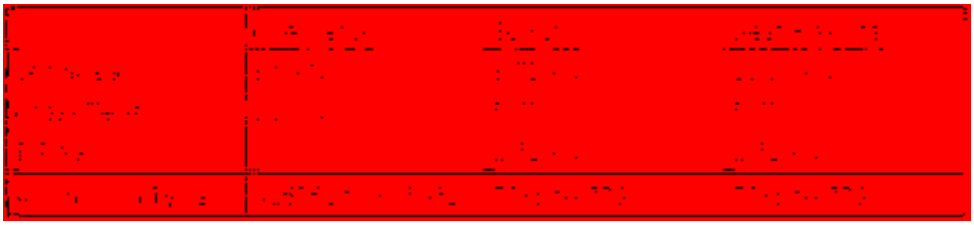

Clinched joints are significantly lower in strength than an FBJ joint in all tests. While clinching does not surpass FBJ in strength it does have its advantages. Clinching is extremely cheap and uses no consumable parts which makes it an attractive alternative if strength is not the primary concern.

4.7.3 FBJ Comparison to Self Piercing Rivets

SPR joints were formed using two pieces of 2mm thick AA5754 by Wang et al. Joints were tested in the lap shear, cross tension and t-peel methods. Comparison results can be found in Table 4-10: Comparison of SPR and FBJ Results

Table 4-10: Comparison of SPR and FBJ Results

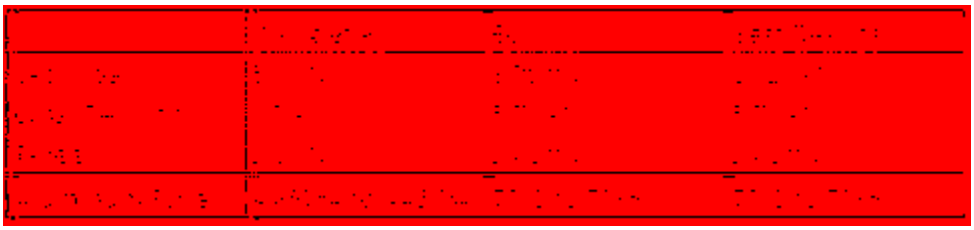

SPR joint strengths approached those found in this research, however were not able to surpass them in any category. Most notably the SPR t-peel sample came the closest coming within 0.5 kN. SPR is an economical alternative to welding and is similar in many regards to

FBJ. Both use a consumable in their process and both cause roughly the same amount of deformation to metals being joined. FBJ does have the advantage of strength, however producing significantly higher results.

4.7.4 FBJ Comparison to the Traditional FBJ Process

The traditional FBJ process uses a steel bit to join a single piece of aluminum to steel coupon. The process uses a consumable bit and the steel coupon acts as a backing to which the nut can attach. The most recent research regarding this topic was done by Shirley who joined a 2 mm thick AA7085 coupon to a GADP 1180 steel coupon by use of a consumable bit. Results can be seen in Table 4-11: Comparison of Traditional FBJ and FBJ Results (Shirley, 2018).

Table 4-11: Comparison of Traditional FBJ and FBJ Results

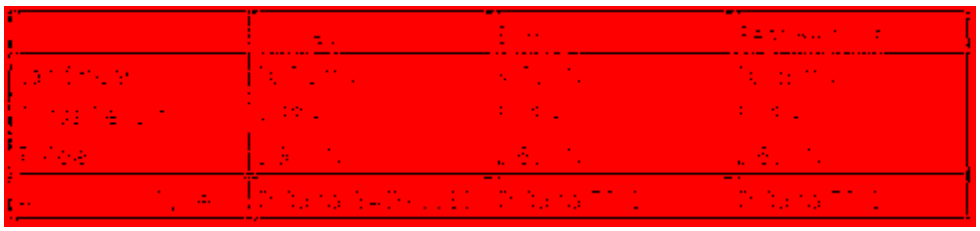

The traditional FBJ process does exceed the FBJ process used in this research in the lap shear joint configuration, however falls short in all other categories. Both FBJ processes have relatively the same advantages and disadvantages, however there are a few worth citing specifically. The tradition FBJ process does not produce welds as strong as those produced in this research's FBJ process, however, it does have the distinct advantage of not needing to use a steel nut as backing. Additionally, the traditional process has only been tested and developed for joining relatively thin working pieces; as such the drilling phase has not been as large of a focus.

5 CONCLUSION AND RECOMMENDATIONS

5.1 Summary

The objective of this research was to explore new applications and variants of the FBJ process. Specifically this research looked at joining two similar metals together with a steel bit and a steel nut backing. The major differences between this research and research that has already been completed was the use of a steel nut rather than the second coupon to form the weld. A second major difference is that the consumable bit has to pierce through a thicker amount of material prior to beginning the welding phase.

This research looked at three independent variables and how their influence affected peak weld strength. The three variables were quantity of flutes, bit head to shank diameter ratio and bit tip surface area. Multiple bits were designed to test each of these three variables. Tests were conducted in a DOE fashion to determine how they influenced overall peak weld strength in isolation. One bit variant was designed to test interaction between quantity of flutes and bit shank diameter, however reliable results were unobtainable due to the dramatically decreased peak weld strength from significantly reduced surface area.

All bit variants were tested in three standard automotive tests, lap shear, cross tension and t-peel. The standard automotive tests of corrosion and fatigue were not investigated. Data was gathered and results were analyzed and presented.

5.2 Conclusions

The various bit designs were designed around three hypotheses. Specifically:

1. Increasing number of flutes, to a point, will have a positive impact on peak weld strength due to the improved ability of the bit to clear chips, after which the effect will be null or even negative.
2. Decreasing bit shank diameter, to a point, will have a positive impact on peak weld strength due to the bit having to cut through less material mass prior to the welding phase. After the shank diameter inflection point has been reached it will have a deteriorating impact on peak weld strength.
3. There is an optimal ratio between consumable bit head diameter and consumable bit tip surface area that will lead to the greatest amount of peak weld strength.

Each hypothesis will be discussed further as to whether or not the data supported or rejected it.

5.2.1 Hypothesis #1 – Flute Quantity

It was hypothesized that increasing number of flutes, to a point, will have a positive impact on peak weld strength due to the improved ability of the bit to clear chips, after which the effect will be null or even negative.

This hypothesis was accepted. In lap shear tests, peak weld strength improved when moving from zero to two flutes, however, a measurably significant difference was not observed by increasing the number of flutes to three. In the lap shear configuration it would seem that two flutes is the optimal choice.

Cross tension tests showed a significant increase in peak weld strength when increasing flute count from two to three, indicating an ideal number of three or more flutes. Surface area results indicated that a decrease in surface area eventually led to a decrease in overall peak weld strength. Continuing to increase flute count would continue to decrease surface area which would eventually lead to a decrease in peak weld strength.

T-peel tests were not statistically significant, so it is difficult to say for certain what the optimal flute number is. The relatively low P value, coupled with the observed data of a switching in failure mode from HPT to NTO provides evidence that supports the hypothesis that increasing number of flutes did add strength to a local region of the joint. Bit head strength increased with addition of flute and so it is theorized that adding flutes in the t-peel configuration added strength to the effect that the head region was no longer the weakest link in the joint.

In all, this hypothesis is accepted.

5.2.2 Hypothesis #2 – Shank Diameter

It was hypothesized that decreasing bit shank diameter, to a point, will have a positive impact on peak weld strength due to the bit having to cut through less material mass prior to the welding phase. After the shank diameter inflection point has been reached it will have a deteriorating impact on peak weld strength.

This theory was accepted. Lap shear tests alone were not conclusive in their evidence. Higher peak strengths were achieved by the largest of the bit designs and then dropped off as the bit shank diameter decreased. It is believed that had bit variants of a larger diameter been tested a bell shaped curve would have appeared in the results. Results from the surface area analysis support this. In this analysis, a bell shaped curve appeared in our analysis with the smallest and

largest bit diameter forming either tail providing evidence that decreasing bit diameter to a point increases peak weld strength. Additionally evidence was found that smaller diameter bits had less coupon deformation supporting the idea that the less material the bit needs to push through the better the peak weld strength.

Cross tension results also supported this theory. Decreasing bit diameter led to improved peak weld strengths. Additionally, it changed the failure mode indicating a decreased diameter strengthened the bit head local area. Continuing to decrease bit diameter was shown in the surface area tests to eventually lead to a decrease in overall peak weld strength.

T-peel results were again not found to be statistically significant. As with other trials, observed results of failure mode switch as diameter decreased does indicate a strengthening of the local region of the bit head with decreasing diameter. In all, this hypothesis was accepted.

5.2.3 Hypothesis #3 – Optimal Head to Surface Area Ratio

It was hypothesized that there is an optimal ratio between consumable bit head diameter and consumable bit tip surface area that will lead to the greatest amount of peak weld strength.

This hypothesis was accepted. Lap shear, cross tension and t-peel tests all showed a distinct bell curve when comparing surface area to peak weld strength. There is a distinct strength tradeoff between two local areas of the joint, specifically the bit head area and the bit-nut intersection. The larger the surface area in relation to the head diameter, the stronger the bit-nut intersection and the weaker the bit head area. The results indicate that there is an optimal single surface area for each of the three testing configurations. In all, this hypothesis was accepted.

5.3 Recommendations

As this branch of FBJ research is in its infancy, there are many areas of opportunity where research could be valuable. Such areas include:

1. Nut design. Reducing the size of the hex nut used in this FBJ process is a major area of opportunity. A reduction in diameter and thickness are both thought to be possible. Additionally, nut shape and design should be considered further.
2. Weld optimization. This research found weld settings that were sufficient to test the different bit designs produced. Optimizing weld parameter, as well as material choice could potentially have a huge impact on increasing peak weld strength.
3. Other testing. Fatigue and corrosion testing were not considered in this research. While strength data is extremely important to any joining process, understanding of how the joint performs in fatigue and corrosive environments is equally important.

These are just a few of the potential areas where further research would be found valuable. Additionally replication of this research and gathering more data sets would be found valuable.

REFERENCES

Aslanlar, S. (2006, 09). The effect of nucleus size on mechanical properties in electrical resistance spot welding of sheets used in automotive industry. *Materials & Design, 27*(2), 125-131. doi:10.1016/j.matdes.2004.09.025

Chen, C., Zhao, S., Han, X., Cui, M., & Fan, S. (2016, 08). Investigation of the height-reducing method for clinched joint with AL5052 and AL6061. *International Journal of Advanced Manufacturing Technology, 89*, 2269-2276. doi:10.1007/s00170-016-9266-0

Deptula, L., & Noah, A. (2015). Estimating the Cost Impact of Lightweighting Automotive Closures. *SAE Technical Paper 2015-01-0581*. doi:10.4271/2015-01-0581

DuPont. (2014). DuPont-Sponsored Survey: Lightweighting Leads Automotive Fuel Efficiency Technologies. Retrieved from http://www.prweb.com/pdfdownload/12074138.pdf

Florea, R., Solanki, K., Bammann, D., Baird, J., Jordan, J., & Castanier, M. (2012, 02). Resistance spot welding of 6061-T6 aluminum: Failure loads and deformation. *Materials & Design, 34*, 624-630. doi:10.1016/j.matdes.2011.05.017

Han, L., Thornton, M., & Shergold, M. (2010, 03). A comparison of the mechanical behavior of self-piercing riveted and resistance spot welded aluminium sheets for the automotive industry. *Materials & Design, 31*(3), 1457-1467. doi:10.1016/j.matdes.2009.08.031

Hao, B., Osman, K., Boomer, D., & Newton, C. (1996, 01). Development in Characterization of Resistance Spot Welding of Aluminum. *Welding Research*, 1-8. Retrieved from http://files.aws.org/wj/supplement/WJ_1996_01_s1.pdf

He, X., Xing, B., Zeng, K., Gu, F., & Ball, A. (2013). Numerical and experimental investigations of self-piercing riveting. *International Journal of Advanced Manufacturing Technology, 69*, 715-721. doi:10.1007/s00170-013-5072-0

He, X., Zhao, L., Yang, H., Xing, B., Wang, Y., Deng, C., . . . Ball, A. (2014, 11). Investigations of strength and engery absorption of clinched joints. *Computational Materials Science, 94*, 58-65. doi:10.1016/j.commatsci.2014.01.056

Lim, Y., Squires, L., Pan, T., Miles, M., Song, G., Wang, Y., & Feng, Z. (2015, March 15). Study of mechanical joint strength of aluminum alloy 7075-T6 and dual phase steel 980 welded by friction bit joining and weld-bonding under corrosion medium. *Materials & Design, 69*, 37-43. Retrieved from https://www.sciencedirect.com/science/article/pii/S0261306914010346#b0070

Miles, M., Kohkonen, K., Packer, S., Steel, R., Siemssen, B., & Sato, Y. (2009). Solid state spot joining of sheet materials using consumable bit. *Science and Technology of Welding and Joining, 14*(1), 72-77. doi:10.1179/136217108X341193

Nied, H. (1984). The finite element modeling of the resistance spot welding process. *Weld. J., 63*(4), 123.

Pereira, A., Ferreira, J., Loureiro, A., Costa, J., & Bartolo, P. (2009, 11). Effect of process parameters on the strength of resistance spot weld in 6082-T6 aluminium alloy. *Materials & Design, 31*(5), 2454-2463. doi:10.1016/j.matdes.2009.11.052

Porcaro, R., Hanssen, A., Langseth, M., & Aalberg, A. (2006, 01). Self-piercing riveting process: An experimental and numerical investigation. *Journal of Materials Processing Technology, 171*(1), 10-20. doi:10.1016/j.jmatprotec.2005.05.048

Shirley, K. (2018). Toward a Production Ready FBJ Process for joining Dissimilar Combinations of GADP 1180 Steel and AA 7085-T76. *All Thesis and Dissertations*, 6694. Retrieved from https://scholarsarchive.byu.edu/etd/6694

Squires, L., Lim, Y., Miles, M., & Feng, Z. (2015, 01). Mechanical properties of dissimilar metal joints composed of DP 980 steel and AA 7075-T6. *Science and Technology of Welding and Joining, 20*(3), 242-248. doi:10.1179/1362171815Y.0000000013

Stein, L., & Dilthey, U. (2006, April). Multimaterial car body design: challenge for welding and joining. *Science & Technology of Welding & Joining, 11*(2), 135-142. doi:10.1179/174329306X85967

Sun, B., Stephens, E., Davies, R., Khaleel, M., & Spinella, D. (2004, 11). Effects of Fusion Zone Size on Failure Modes and Static Strength of Aluminum Resistance Spot Welds. *Welding Research*, 308-318.

Varis, J., & Lepisto, J. (2003, 08). A simple testing-based procedure and simulation of the clinching process using finite element analysis for establishing clinching parametersf. *Thin-Walled Structures, 41*(8), 691-709. doi:10.1016/S0263-8231(03)00026-0

Wang, B., Hao, C., Zhang, J., & Zhang, H. (2005, 04). A New Self-Piercing Riveting Process and Strength Evaluation. *Journal of Manufacturing Science Engineering, 128*(2), 580-587. doi:10.1115/1.2137746

APPENDICES

APPENDIX A – OKUMA LATHE CODE

ECHO6

DEF WORK

PS LC,[-10,0],[10,05]

END

DRAW

G00 X20 Z20

G50 S4500 (G50 - Max spindle speed)

X.55 Z.2 S1000 T020202 M03 M42 M08 M42 (SET TOOL 2)

G96 S600 (G96 - constant cutting speed on)

G85 NLAP1 D.05 F.015 U.01 W.004 (G85 - rough turning operation)

NLAP1 G81 (G81 - start longitudinal shape design)

G00 X0. (DEFINE PROFILE)

G01 Z0.052 G42 F.003 (G42 - tool nose compensation right)

X.05 Z.052

X.05 Z0.02

X.280 Z-.01

G76X.300 Z-.290 L.0425 (G76 - auto rounding)

X.385

Z-.576 (L-CHANGE 2: Z=TOTAL CLEANED UP LENGTH)

G40 X.40 (cancel tool nose radius compensation)

G80 (End of shape designation)

G00 Z.1

G96 S600

G87 NLAP1

G00 Z.1

G00 X20 Z20 M12 M146

G95 M109 (FEED IN/REV - CANCEL M110)

G97 S1000 M03

(CUT OFF PIN)

G00 X20 Z20 (HOME)

X.1 Z0.050 S1000 T080808 M03 M08 (SET PARTING TOOL)

G97 S1200

G01 X-.2 F.003 (CUT OFF)

G00 X.6

(FINISH PART OFF)

Z-.473 (LENGTH CHANGE 3: PART OFF LOCATION, <CHANGE 2)

G01 X-.1 F.002 (PART OFF)

G00 X.6

X20 Z20

M02

ECHO9

DEF WORK

PS LC,[-10,0],[10,05]

END

DRAW

G00 X20 Z20

G50 S4500 (G50 - Max spindle speed)

X.55 Z.2 S1000 T020202 M03 M42 M08 M42 (SET TOOL 2)

G96 S600 (G96 - constant cutting speed on)

G85 NLAP1 D.05 F.015 U.01 W.004 (G85 - rough turning operation)

NLAP1 G81 (G81 - start longitudinal shape design)

G00 X0. (DEFINE PROFILE)

G01 Z0.052 G42 F.003 (G42 - tool nose compensation right)

X.05 Z.052

X.05 Z0.02

X.280 Z-.01

G76X.300 Z-.240 L.0425 (G76 - auto rounding)

X.385

Z-.526 (L-CHANGE 2: Z=TOTAL CLEANED UP LENGTH)

G40 X.40 (cancel tool nose radius compensation)

G80 (End of shape designation)

G00 Z.1

G96 S600

G87 NLAP1

G00 Z.1

(HIP WELLS AND TEETH)

G97 S1000

N500 G00 X20 Z20 M05

M110 (C-AXIS JOINT)

M146 M15 (C-AXIS UNCLAMP)

M110 (START)

M15

G94 X.75 Z.3 T1212 SB=3000 M13 M08

X.7 Z.05

G190 X.12 Z-.265 C0 K.060 D.05 W.015 E5.0 F2.5 M211 M213

C180

G180

(CUT FACE TAPERS)

G00 X20 Z20 M12

M109 M146

M110 M16 G94 X.573 Z.4 T0606

Z.065 SB=1200 M13

G185 G95 X.05 Z.035 C325 F.07 SA=2.0 (CUT TAPERS)

G180

G00 X.573 Z.4

C180

Z.065

G185 X.05 Z.035 C145 F.070 SA=2.0

G180

G00 X20 Z20 M12 M146

G95 M109 (FEED IN/REV - CANCEL M110)

G97 S1000 M03

(CUT OFF PIN)

G00 X20 Z20 (HOME)

X.1 Z0.050 S1000 T080808 M03 M08 (SET PARTING TOOL)

G97 S1200

G01 X-.2 F.003 (CUT OFF)

G00 X.6

(FINISH PART OFF)

Z-.423 (LENGTH CHANGE 3: PART OFF LOCATION, <CHANGE 2)

G01 X-.1 F.002 (PART OFF)

G00 X.6

X20 Z20

ECH10

DEF WORK

PS LC,[-10,0],[10,05]

END

DRAW

G00 X20 Z20

G50 S4500 (G50 - Max spindle speed)

X.55 Z.2 S1000 T020202 M03 M42 M08 M42 (SET TOOL 2)

G96 S600 (G96 - constant cutting speed on)

G85 NLAP1 D.05 F.015 U.01 W.004 (G85 - rough turning operation)

NLAP1 G81 (G81 - start longitudinal shape design)

G00 X0. (DEFINE PROFILE)

G01 Z0.052 G42 F.003 (G42 - tool nose compensation right)

X.05 Z.052

X.05 Z0.02

X.280 Z-.01

G76X.300 Z-.240 L.0425 (G76 - auto rounding)

X.385

Z-.526 (L-CHANGE 2: Z=TOTAL CLEANED UP LENGTH)

G40 X.40 (cancel tool nose radius compensation)

G80 (End of shape designation)

G00 Z.1

G96 S600

G87 NLAP1

G00 Z.1

(HIP WELLS AND TEETH)

G97 S1000

N500 G00 X20 Z20 M05

M110 (C-AXIS JOINT)

M146 M15 (C-AXIS UNCLAMP)

M110 (START)

M15

G94 X.75 Z.3 T1212 SB=3000 M13 M08

X.7 Z.05

G190 X.12 Z-.265 C0 K.060 D.05 W.015 E5.0 F2.5 M211 M213

C120

C240

G180

(CUT FACE TAPERS)

G00 X20 Z20 M12

M109 M146

M110 M16 G94 X.573 Z.4 T0606

```
Z.065 SB=1200 M13

G185 G95 X.05 Z.035 C0 F.1 SA=2.0 (CUT TAPERS)

G180


G00 X.573 Z.4

C120

Z.065

G185 X.05 Z.035 C120 F.1 SA=2.0

G180


G00 X.573 Z.4

C120

Z.065

G185 X.05 Z.035 C240 F.1 SA=2.0

G180


G00 X20 Z20 M12 M146

G95 M109 (FEED IN/REV - CANCEL M110)
```

G97 S1000 M03

(CUT OFF PIN)

G00 X20 Z20 (HOME)

X.1 Z0.050 S1000 T080808 M03 M08 (SET PARTING TOOL)

G97 S1200

G01 X-.2 F.003 (CUT OFF)

G00 X.6

(FINISH PART OFF)

Z-.423 (LENGTH CHANGE 3: PART OFF LOCATION, <CHANGE 2)

G01 X-.1 F.002 (PART OFF)

G00 X.6

X20 Z20

M02

ECH11

DEF WORK

PS LC,[-10,0],[10,05]

END

DRAW

G00 X20 Z20

G50 S4500 (G50 - Max spindle speed)

X.55 Z.2 S1000 T020202 M03 M42 M08 M42 (SET TOOL 2)

G96 S600 (G96 - constant cutting speed on)

G85 NLAP1 D.05 F.015 U.01 W.004 (G85 - rough turning operation)

NLAP1 G81 (G81 - start longitudinal shape design)

G00 X0. (DEFINE PROFILE)

G01 Z0.052 G42 F.003 (G42 - tool nose compensation right)

X.05 Z.052

X.05 Z0.02

X.220 Z-.01

G76X.240 Z-.240 L.0425 (G76 - auto rounding)

X.385

Z-.526 (L-CHANGE 2: Z=TOTAL CLEANED UP LENGTH)

G40 X.40 (cancel tool nose radius compensation)

G80 (End of shape designation)

G00 Z.1

G96 S600

G87 NLAP1

G00 Z.1

(HIP WELLS AND TEETH)

G97 S1000

N500 G00 X20 Z20 M05

M110 (C-AXIS JOINT)

M146 M15 (C-AXIS UNCLAMP)

M110 (START)

M15

G94 X.75 Z.3 T1212 SB=3000 M13 M08

X.7 Z.05

G190 X.096 Z-.265 C0 K.060 D.05 W.015 E5.0 F2.5 M211 M213

C180

G180

(CUT FACE TAPERS)

G00 X20 Z20 M12

M109 M146

M110 M16 G94 X.573 Z.4 T0606

Z.065 SB=1200 M13

G185 G95 X.05 Z.035 C325 F.07 SA=2.0 (CUT TAPERS)

G180

G00 X.573 Z.4

C180

Z.065

G185 X.05 Z.035 C145 F.070 SA=2.0

G180

G00 X20 Z20 M12 M146

G95 M109 (FEED IN/REV - CANCEL M110)

G97 S1000 M03

(CUT OFF PIN)

G00 X20 Z20 (HOME)

X.1 Z0.050 S1000 T080808 M03 M08 (SET PARTING TOOL)

G97 S1200

G01 X-.2 F.003 (CUT OFF)

G00 X.6

(FINISH PART OFF)

Z-.423 (LENGTH CHANGE 3: PART OFF LOCATION, <CHANGE 2)

G01 X-.1 F.002 (PART OFF)

G00 X.6

X20 Z20

M02

ECH12

DEF WORK

PS LC,[-10,0],[10,05]

END

DRAW

G00 X20 Z20

G50 S4500 (G50 - Max spindle speed)

X.55 Z.2 S1000 T020202 M03 M42 M08 M42 (SET TOOL 2)

G96 S600 (G96 - constant cutting speed on)

G85 NLAP1 D.05 F.015 U.01 W.004 (G85 - rough turning operation)

NLAP1 G81 (G81 - start longitudinal shape design)

G00 X0. (DEFINE PROFILE)

G01 Z0.052 G42 F.003 (G42 - tool nose compensation right)

X.05 Z.052

X.05 Z0.02

X.220 Z-.01

G76X.240 Z-.240 L.0425 (G76 - auto rounding)

X.385

Z-.526 (L-CHANGE 2: Z=TOTAL CLEANED UP LENGTH)

G40 X.40 (cancel tool nose radius compensation)

G80 (End of shape designation)

G00 Z.1

G96 S600

G87 NLAP1

G00 Z.1

(HIP WELLS AND TEETH)

G97 S1000

N500 G00 X20 Z20 M05

M110 (C-AXIS JOINT)

M146 M15 (C-AXIS UNCLAMP)

M110 (START)

M15

G94 X.75 Z.3 T1212 SB=3000 M13 M08

X.7 Z.05

G190 X.096 Z-.265 C0 K.060 D.05 W.015 E5.0 F2.5 M211 M213

C120

C240

G180

(CUT FACE TAPERS)

G00 X20 Z20 M12

M109 M146

M110 M16 G94 X.573 Z.4 T0606

Z.065 SB=1200 M13

G185 G95 X.05 Z.035 C0 F.1 SA=2.0 (CUT TAPERS)

G180

G00 X.573 Z.4

C120

Z.065

G185 X.05 Z.035 C120 F.1 SA=2.0

G180

G00 X.573 Z.4

C120

Z.065

G185 X.05 Z.035 C240 F.1 SA=2.0

G180

G00 X20 Z20 M12 M146

ECH13

DEF WORK

PS LC,[-10,0],[10,05]

END

DRAW

G00 X20 Z20

G50 S4500 (G50 - Max spindle speed)

X.55 Z.2 S1000 T020202 M03 M42 M08 M42 (SET TOOL 2)

G96 S600 (G96 - constant cutting speed on)

G85 NLAP1 D.05 F.015 U.01 W.004 (G85 - rough turning operation)

NLAP1 G81 (G81 - start longitudinal shape design)

G00 X0. (DEFINE PROFILE)

G01 Z0.052 G42 F.003 (G42 - tool nose compensation right)

X.05 Z.052

X.05 Z0.02

X.250 Z-.01

G76X.270 Z-.240 L.0425 (G76 - auto rounding)

X.385

Z-.526 (L-CHANGE 2: Z=TOTAL CLEANED UP LENGTH)

G40 X.40 (cancel tool nose radius compensation)

G80 (End of shape designation)

G00 Z.1

G96 S600

G87 NLAP1

G00 Z.1

(HIP WELLS AND TEETH)

G97 S1000

N500 G00 X20 Z20 M05

M110 (C-AXIS JOINT)

M146 M15 (C-AXIS UNCLAMP)

M110 (START)

M15

G94 X.75 Z.3 T1212 SB=3000 M13 M08

X.7 Z.05

G190 X.108 Z-.265 C0 K.060 D.05 W.015 E5.0 F2.5 M211 M213

C180

G180

(CUT FACE TAPERS)

G00 X20 Z20 M12

M109 M146

M110 M16 G94 X.573 Z.4 T0606

Z.065 SB=1200 M13

G185 G95 X.05 Z.035 C325 F.07 SA=2.0 (CUT TAPERS)

G180

G00 X.573 Z.4

```
C180

Z.065

G185 X.05 Z.035 C145 F.070 SA=2.0

G180

G00 X20 Z20 M12 M146

G95 M109 (FEED IN/REV - CANCEL M110)

G97 S1000 M03

(CUT OFF PIN)

G00 X20 Z20 (HOME)

X.1 Z0.050 S1000 T080808 M03 M08 (SET PARTING TOOL)

G97 S1200

G01 X-.2 F.003    (CUT OFF)

G00 X.6

(FINISH PART OFF)

Z-.423   (LENGTH CHANGE 3: PART OFF LOCATION, <CHANGE 2)

G01 X-.1 F.002    (PART OFF)

G00 X.6

X20 Z20

M02
```

APPENDIX B – SURFACE AREA CALCULATIONS AND EQUATION

Surface Area calculations were made using one of two methods. The decision on what method to use was depended on the depth of cut of the flute. If the full diameter of the drill bit sunk into the consumable bit shank, method 1 was used. If the full diameter of the drill did not enter the consumable bit shank then method 2 was used. See figure below.

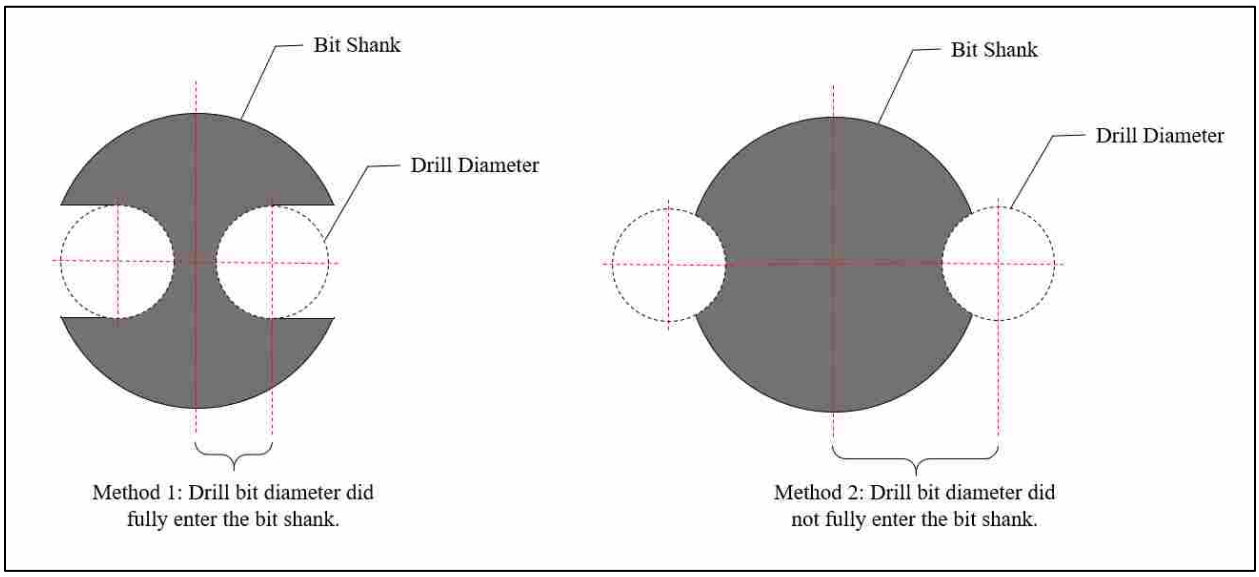

To determine whether or not the full diameter of the drill bit had fully engaged in the consumable bit shank a calculation was performed. Because the diameter of both the drill bit and the consumable bit were known, angle, θ, could be calculated for the maximum b. If θ did not meet or exceed this maximum θ, then it was known that the full drill bit diameter did not fully engage as seen in the figure below.

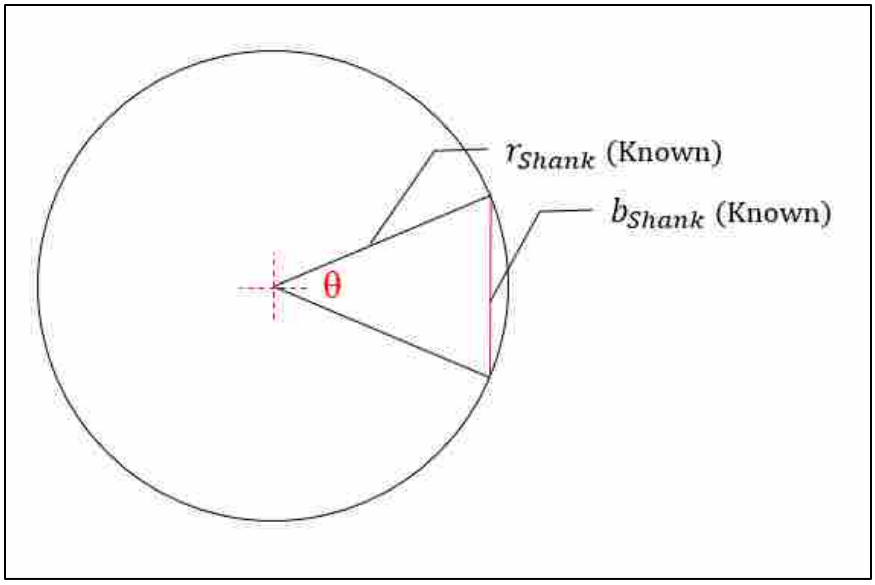

$$a^2 = b^2 + c^2 - 2bc\cos A$$

Method 1

In method 1 the surface area that is removed by the cutting of the flutes is subtracted from the total area of the bit as seen in the equation below.

$$Surface\ Area = A\ - 2(B + C + D)$$

The area of flute was calculated by dividing the cut into three sections: Section B, which was the half circle created by the drill bit at the end of the cut, Section C, which extended from the point of where the center of the drill bit stopped back to the secant line which runs from edge to edge of the entry cut, and Section D was the segment that runs from the secant to the edge of the diameter of the consumable bit shank. All three sections can be seen in the figure below.

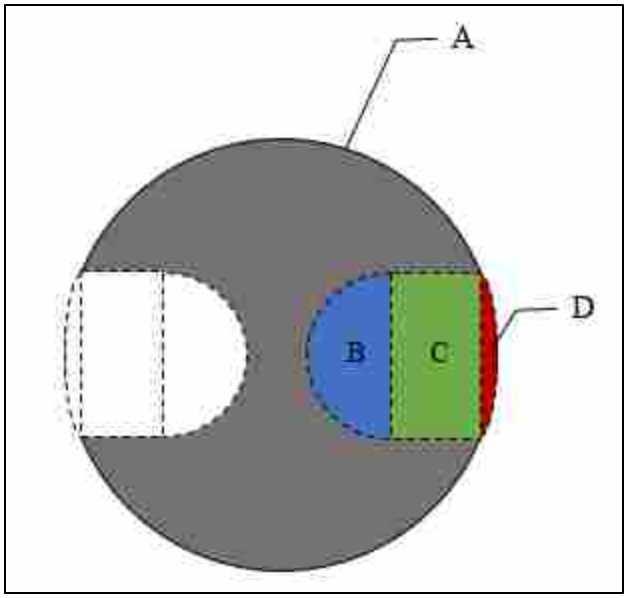

Section A

Section A was a simple calculation using the equation show below, where r was the radius of the consumable bit.

$$A = \pi r^2$$

Section B

Section B was also a simple calculation of a semicircle. The equation is found below. In this case r was the radius of the drill bit. A 1/8th in drill bit was used to make the flutes.

$$A = \frac{\pi r^2}{2}$$

Section C

Section C was calculated using the equation below.

$$A = bw$$

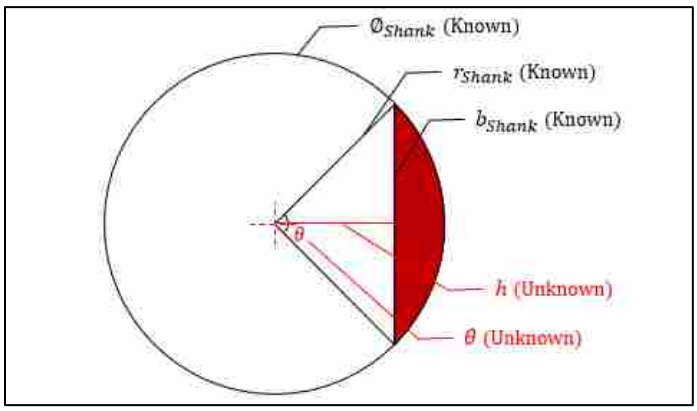

Here b was the diameter of the drill bit and w was calculated subtracting the known depth of cut from h. The distance h was calculated using the law of cosines.

First θ needed to be calculated, seen in the figure above. The angle θ was calculated by using the law of cosines as all three sides were of known length. Two were the radius of the consumable bit shank and the secant line was equal to the diameter of the drill bit.

Once θ was known, it was cut in half to produce the interior angle Φ as seen in the figure below. Using the equation below, all interior angles could be calculated.

$$180 = \angle A + \angle B + \angle C$$

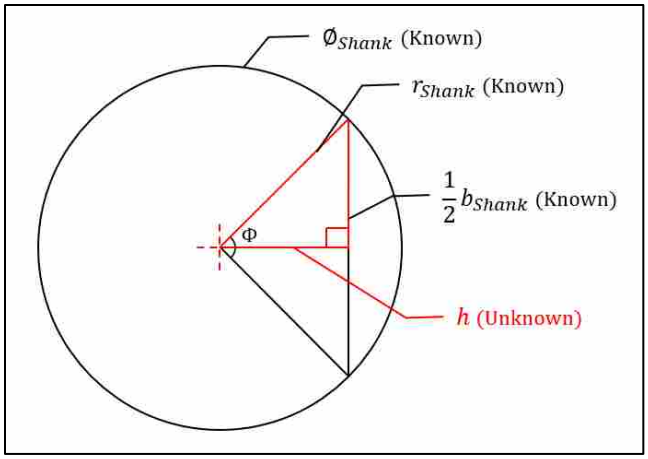

The law of cosines was then used to determine the length of h.

Section D

Section D was calculated using the equation shown below. The figure below shows a graphical depiction of the variables. For this equation b was the diameter of the drill bit, r was the radius of the shank and θ and h were calculated in Section C.

$$A = (\pi r^2) * \left(\frac{\theta}{360}\right) - \frac{1}{2}bh$$

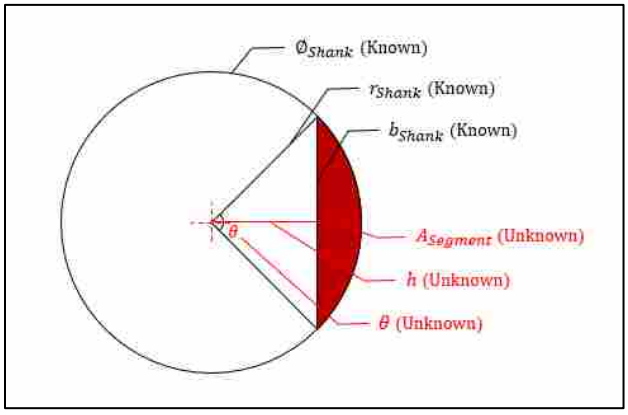

Method 2

The method 2 calculation was similar to Method 1, however it did not include Section C, the box area as seen in the figure below

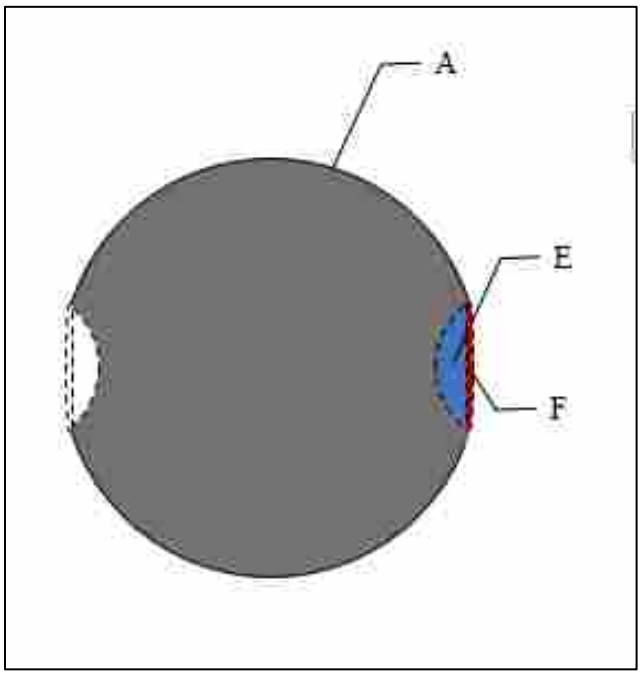

Once the areas for Sections E and F had been calculated, they were backed out of the total area of the bit shank, Section A to compute the total bit tip area.

Section A

Section A was the same as was calculated earlier in 7.1.1 Section A.

Section E

Section E was calculated using the equation for the area of a segment. Here r was the radius of the bit shank while θ, b and h were unknown.

The distance b was calculated first and was equal to the length of the segment. Using Pythagoreans equation, shown below, the length of h or the segment was able to be found. In this case c represented h, and a and b were the radii of the consumable bit shank and the drill bit shank respectively.

$$a^2 + b^2 = c^2$$

Once h was found, θ was able to be calculated using the law of cosines. For this equation, a was h, θ was A, and b and c were the radius of the consumable bit shank.

Once θ was known the equation for the area of a segment was able to be used to calculate the area of Section E.

Section F

Section F was calculated using the equation for the area of a segment. θ was calculated in Section E as were b and h.

APPENDIX C – RAW DATA SETS AND RESULTS

ECHO6 Results					
	Sample	Peak (N)	Ext (mm)	Primary Failure	Secondary Failure
LAP SHEAR	1	9,200	3.78	HPT	
	2	11,200	3.22	HPT	
	3	6,467	3.70	HPT	
	4	8,086	3.89	HPT	
	5	6,427	3.51	HPT	
	6	9,296	3.45	HPT	
	7	4,003	3.56	HPT	
	8	8,687	4.04	HPT	
	9	7,388	4.45	HPT	
	10	11,623	4.09	NTO	
	11	5,529	3.43	HPT	
	12	6,707	4.22	HPT	
	13	8,647	4.11	HPT	
	14	8,109	3.40	HPT	
	15	7,014	3.28	HPT	

ECHO9 Results					
	Sample	Peak (N)	Ext (mm)	Primary Failure	Secondary Failure
LAP SHEAR	1	9,808	3.78	HPT	NTO
	2	10,448	3.22	NTO	HPT
	3	10,715	3.70	NTO	HPT
	4	10,680	3.89	HPT	NTO
	5	10,257	3.51	NTO	HPT
	6	9,857	3.45	HPT	NTO
	7	9,634	3.56	HPT	NTO
	8	10,462	4.04	HPT	NTO
	9	10,626	4.45	HPT	NTO
	10	10,484	4.09	HPT	NTO
	11	10,030	3.43	HPT	NTO
	12	10,426	4.22	HPT	NTO
	13	9,941	4.11	HPT	NTO
	14	10,146	3.40	NTO	HPT
	15	9,981	3.28	NTO	HPT

ECHO9 Results					
CROSS TENSION	Sample	Peak (N)	Ext (mm)	Primary Failure	Secondary Failure
	1	4,351	12.85	HPT	
	2	3,806	10.39	HPT	
	3	4,284	11.91	HPT	
	4	4,087	11.4	HPT	
	5	3,708	10.24	HPT	
	6	3,281	9.34	HPT	
	7	3,268	9.83	HPT	
	8	3,964	11.27	HPT	
	9	3,808	10.97	HPT	
	10	4,193	13.32	HPT	
	11	3,968	12.01	HPT	
	12	3,446	10.31	HPT	
	13	3,975	12.62	HPT	
	14	4,586	15.49	HPT	
	15	3,331	10.13	HPT	
	16	5,075	16.56	HPT	

ECHO9 Results					
T-PEEL	Sample	Peak (N)	Ext (mm)	Primary Failure	Secondary Failure
	1	2,370	8.31	HPT	
	2	1,875	5.68	HPT	
	3	2,427	7.50	HPT	
	4	2,632	7.8	HPT	
	5	2,145	6.6	HPT	
	6	2,500	7.39	HPT	
	7	2,476	7.37	HPT	
	8	2,636	7.4	HPT	
	9	2,121	5.77	HPT	
	10	2,564	7.18	HPT	
	11	2,617	7.44	HPT	
	12	2,758	9.25	HPT	
	13	1,936	5.56	HPT	
	14	2,901	8.13	HPT	
	15	2,529	7.16	HPT	
	16	2,724	10.16	HPT	

ECH10 Results					
LAP SHEAR	Sample	Peak (N)	Ext (mm)	Primary Failure	Secondary Failure
	1	10,052	5.511	HPT	NTO
	2	9,145	2.511	HPT	NTO
	3	9,256	2.97	NTO	HPT
	4	10,115	3.75	HPT	NTO
	5	10,115	3.68	NTO	HPT
	6	9,977	3.3	NTO	HPT
	7	9,697	3.07	NTO	HPT
	8	9,643	2.69	HPT	NTO
	9	9,835	3.58	HPT	NTO
	10	9,754	3.79	NTO	HPT
	11	10,008	3.68	HPT	NTO
	12	9,746	3.78	HPT	NTO
	13	10,462	3.83	HPT	NTO
	14	9,768	3.93	HPT	NTO
	15	9,625	2.71	HPT	NTO
	16	9,247	3.32	HPT	NTO

ECH10 Results					
CROSS TENSION	Sample	Peak (N)	Ext (mm)	Primary Failure	Secondary Failure
	1	6,027	19.48	HPT	
	2	Sample Tested Incorrectly			
	3	6,183	18.77	HPT	NTO
	4	6,196	22.52	HPT	
	5	5,444	18.41	NTO	
	6	6,089	18.82	NTO	HPT
	7	4,959	15.03	NTO	
	8	5,373	15.87	NTO	HPT
	9	6,040	19.6	HPT	
	10	5,831	19.48	HPT	
	11	5,724	22.65	HPT	
	12	6,734	23.59	HPT	
	13	5,933	17.95	HPT	
	14	5,600	18.21	HPT	
	15	4,577	12.67	HPT	
	16	5,938	18.28	HPT	NTO

ECH10 Results					
	Sample	Peak (N)	Ext (mm)	Primary Failure	Secondary Failure
T-PEEL	1	2,281	8.94	NTO	
	2	2,255	5.96	NTO	
	3	3,292	11.60	NTO	
	4	2,116	6.93	NTO	
	5	2,236	7.62	NTO	
	6	2,906	8.86	NTO	
	7	2,758	7.54	NTO	
	8	2,524	9.16	NTO	
	9	2,241	7.92	NTO	
	10	2,236	7.72	NTO	
	11	2,849	10.69	NTO	
	12	2,695	7.69	NTO	
	13	3,014	8.58	NTO	
	14	3,084	10.05	NTO	
	15	2,764	7.87	NTO	
	16	2,434	6.52	NTO	

ECH11 Results					
	Sample	Peak (N)	Ext (mm)	Primary Failure	Secondary Failure
LAP SHEAR	1	10,270	3.25	NTO	HPT
	2	9,714	3.93	NTO	HPT
	3	9,679	3.81	NTO	HPT
	4	8,669	3.68	NTO	HPT
	5	10,173	3.22	NTO	HPT
	6	11,080	3.35	NTO	HPT
	7	9,861	2.92	NTO	HPT
	8	9,821	2.81	NTO	HPT
	9	10,715	3.47	HPT	NTO
	10	9,737	2.59	NTO	HPT
	11	9,523	2.31	NTO	HPT
	12	9,768	2.99	NTO	HPT
	13	9,870	2.76	NTO	HPT
	14	10,898	3.68	NTO	HPT
	15	10,408	3.20	NTO	HPT
	16	9,443	2.59	NTO	HPT

ECH11 Results					
CROSS TENSION	Sample	Peak (N)	Ext (mm)	Primary Failure	Secondary Failure
	1	5,093	11.3	NTO	
	2	5,600	14.65	NTO	
	3	6,134	14.70	NTO	
	4	5,586	15.92	NTO	
	5	5,747	15.59	HPT	NTO
	6	4,848	15.57	HPT	
	7	5,248	16.56	NTO	
	8	5,417	17.98	NTO	
	9	5,302	16.73	NTO	
	10	5,351	18.97	NTO	
	11	5,831	24.07	NTO	
	12	5,778	21.66	NTO	
	13	5,907	21.56	NTO	
	14	5,466	16	NTO	
	15	4,420	12.57	NTO	
	16	5,333	17.37	NTO	

ECH11 Results					
T-PEEL	Sample	Peak (N)	Ext (mm)	Primary Failure	Secondary Failure
	1	2,351	8.91	NTO	
	2	1,109	2.92	NTO	
	3	2,330	7.79	NTO	
	4	1,402	4.11	NTO	
	5	2,665	9.47	NTO	
	6	2,923	11.17	NTO	
	7	2,168	8.89	NTO	
	8	2,174	7.77	NTO	
	9	2,050	11.3	NTO	
	10	2,007	6.78	NTO	
	11	2,646	9.06	NTO	
	12	1,813	5.46	NTO	
	13	2,182	6.52	NTO	
	14	2,728	9.24	NTO	
	15	2,576	10.00	NTO	
	16	2,230	8.96	NTO	

ECH12 Results					
LAP SHEAR	Sample	Peak (N)	Ext (mm)	Primary Failure	Secondary Failure
	1	7,126	1.44	NTO	
	2	7,486	1.72	NTO	
	3	8,313	2.36	NTO	
	4	8,269	2.15	NTO	
	5	7,384	2.23	NTO	
	6	6,400	1.24	NTO	
	7	8,803	2.08	NTO	
	8	6,930	3.07	NTO	
	9	7,851	2.15	NTO	
	10	9,105	2.28	NTO	
	11	4,844	1.37	NTO	
	12	5,146	1.32	NTO	
	13	6,658	2.56	NTO	
	14	9,528	2.81	NTO	
	15	8,273	1.95	NTO	
	16	6,587	2.81	NTO	

ECH12 Results					
CROSS TENSION	Sample	Peak (N)	Ext (mm)	Primary Failure	Secondary Failure
	1	3,417	7.62	NTO	
	2	3,523	7.95	NTO	
	3	4,184	10.13	NTO	
	4	3,627	7.79	NTO	
	5	3,551	9.14	NTO	
	6	3,841	8.83	NTO	
	7	3,603	8.2	NTO	
	8	3,434	9.11	NTO	
	9	3,473	7.67	NTO	
	10	3,768	8.15	NTO	
	11	3,668	7.92	NTO	
	12	4,437	11.35	NTO	
	13	3,734	8.45	NTO	
	14	3,730	8.76	NTO	
	15	4,188	11.60	NTO	
	16	3,676	10.21	HPT	

ECH12 Results					
T-PEEL	Sample	Peak (N)	Ext (mm)	Primary Failure	Secondary Failure
	1	1,681	6.17	NTO	
	2	2,137	7.08	NTO	
	3	2,340	7.56	NTO	
	4	2,101	6.37	NTO	
	5	1,594	6.88	NTO	
	6	1,658	7.28	NTO	
	7	1,705	8.53	NTO	
	8	1,683	6.93	NTO	
	9	1,755	8.66	NTO	
	10	1,662	7.69	NTO	
	11	1,846	7.69	NTO	
	12	874	3.5	SF	
	13	1,092	4.08	SF	
	14	1,750	7.77	NTO	
	15	2,007	6.88	NTO	
	16	1,645	8.35	NTO	

ECH13 Results					
LAP SHEAR	Sample	Peak (N)	Ext (mm)	Primary Failure	Secondary Failure
	1	9,799	2.05	NTO	
	2	9,594	2.89	NTO	
	3	9,750	2.46	NTO	
	4	9,817	2.51	NTO	
	5	9,590	1.85	NTO	

ECH13 Results					
CROSS TENSION	Sample	Peak (N)	Ext (mm)	Primary Failure	Secondary Failure
	1	6,000	18.69	NTO	
	2	5,484	20.62	NTO	
	3	6,485	22.83	NTO	
	4	5,431	18.87	NTO	
	5	4,959	13.61	NTO	

ECH13 Results					
T-PEEL	Sample	Peak (N)	Ext (mm)	Primary Failure	Secondary Failure
	1	2,149	8.02	NTO	
	2	2,486	8.3	NTO	
	3	2,542	7.84	NTO	
	4	2,639	8.76	NTO	
	5	1,958	5.43	NTO	